Paintable Hybrids with Thermally Stable Dual Emission Composed of Tetraphenylethene-Integrated POSS and MEH-PPV for Heat-Resistant White-Light Luminophores

Masayuki Gon, Satoru Saotome, Kazuo Tanaka* and Yoshiki Chujo

Department of Polymer Chemistry, Graduate School of Engineering, Kyoto University Katsura, Nishikyo-ku, Kyoto 615-8510, Japan

E-mail: tanaka@poly.synchem.kyoto-u.ac.jp

Key words: POSS; dual emission; organic-inorganic hybrid; white-light emission, π-conjugated polymer

Table of Contents

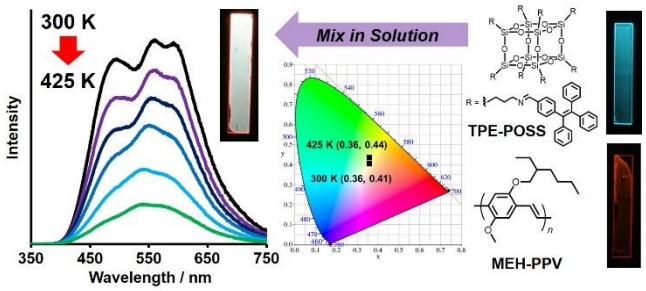

Abstract

Thermally stable dual emission followed by white-light luminescence from hybrid materials is reported. Hybrid films were prepared with a spin-coating method with the mixture solution containing tetraphenylethene (TPE)-integrated polyhedral oligomeric silsesquioxane (POSS) and poly[2-methoxy-5-(2′-ethylhexyloxy)-1,4-phenylene vinylene] (**MEH-PPV**). TPE-tethered POSS (**TPE-POSS**) showed high compatibility with **MEH-PPV**. Therefore, homogeneous films with variable concentrations of **TPE-POSS** were obtained. Owing to well dispersion of rigid silica cubes into matrices, POSS-containing films demonstrated high thermal stability toward molecular rearrangement by annealing as well as pyrolysis, similarly to conventional polymer hybrids. Furthermore, it was found that **TPE-POSS** was able to enhance emission efficiencies probably by suppressing chain aggregation. By modulating introduction ratios of **TPE-POSS**, dual-emission properties followed by white-light luminescence composed of cyan and orange emissions from **TPE-POSS** and **MEH-PPV**, respectively, were accomplished. It should be noted that these color balances can be preserved even in the high temperature region (425 K). Finally, white-light luminescent materials with thermal durability were obtained.

Introduction

Polymeric materials with white-light emission have tremendous attention as a promising platform for realizing paper-type illumination.[1] In principle, combinations of two or three-types of different colors are necessary for generating white light.[2–5] Therefore, in the material design, the key point is to maintain a color balance suitable for white emission. So far, several strategies have been proposed, such as encapsulation into micelles[6–9] or vesicles,[10–12] host-guest interactions,[13–16] fixation into gels,[17–21] arrangement with metal organic frameworks (MOF).[22–28] White-light emission from a single luminophore has been also realized by the assortment of different emission mechanisms.[29–39]

Thermal stability of the emitting material is one of essential factors to fabricate robust devices.[40] In particular, since the material performance consisting of several components is often spoiled by temperature changes due to activation of molecular motion followed by phase separation, it is important not only to realize mixing state but also to maintain original states.[41] Previously, we reported the preparation of thermally and chemically stable hybrids with white-light emission with three-kinds of different luminophores.[42] The light-emitting components were anchored into each component for separating each other and preventing from intermolecular interaction as well as energy transferring. However, due to severe conditions in conventional sol-gel reactions, where polar solvents and acid or base catalysts are required, degradation frequently occurred. Thus, it is still challenging to apply functional polymers in the hybrid formations without degradation of optoelectronic properties and non-specific aggregation. The cohesive forces of π-conjugated polymers are too strong to preserve homogeneous states at the molecular level during hybrid formations.

In order to homogeneously mix π-conjugated polymers and other components, we have focused on polyhedral oligomeric silsesquioxane (POSS).[43–45] POSS is organic–inorganic hybrid molecules consisting of a cubic silica core and organic substituents at eight vertices. The unique three-dimensional structure consisting of organic and inorganic components is regarded as a versatile element-block,[46–49] which is the minimum functional unit including heteroatoms, for producing designable hybrid materials according to the preprogrammed design.[50–64] Indeed, we have constructed homogeneous hybrid materials with π-conjugated polymers based on luminophore-integrated POSS[65] through facile mixing in solution without sol–gel reactions.[66,67] In particular, we found that the dendritic-arranged substituents on POSS led to low crystallinity and high compatibility to π-conjugated polymers. The resulting hybrid materials based on POSS showed high thermal stability and intense emission from π-conjugated polymers owing to light-harvesting effect of the POSS through fluorescence resonance energy transfer (FRET).[66,68]

Herein, in order to obtain thermally stable dual emission leading to white-light emission, we constructed hybrid materials with imino-tetraphenylethene-integrated POSS (**TPE-POSS**) and poly[2-methoxy-5-(2′-ethylhexyloxy)-1,4-phenylene vinylene] (**MEH-PPV**).[69] Tetraphenylethene (TPE) derivatives are well known as a unique luminophore showing aggregation-induced emission (AIE).[70] Since the class of AIE-active molecules is emissive by the restriction of molecular tumbling under condensed conditions, TPE is expected to be an efficient solid-state emissive source.[71] Complementary emission colors with **TPE-POSS** (cyan emission) and **MEH-PPV** (orange emission) have the appropriate relationship for generating white-light emission. In particular, by connecting to the rigid silica cube, solid-state emission properties of

TPE could be greatly enhanced followed by dual emission even in the condensed state with conjugated polymer matrices. Therefore, robust hybrids with white-light emission could be obtained by employing POSS. On the basis of these speculations, we prepared the series of hybrids based on POSS through solution methods and evaluated optical and thermal properties.

Materials and Methods

Materials. Propylamine, potassium *tert*-butoxide (*tert*-BuOK) were purchased from Tokyo Chemical Industry Co, Ltd. Methanol (MeOH), acetone, hexane, chloroform ($CHCl_3$) were purchased from FUJIFILM Wako Pure Chemical Industries, Ltd. and used without purification. Tetrahydrofuran (THF) (FUJIFILM Wako Pure Chemical Industries, Ltd.) and triethylamine (Et_3N) (Kanto Chemical Co., Inc.) were purified by passage through solvent purification columns under N_2 pressure. Octakis(3-aminopropyl) POSS hydrochloride (**Amino-POSS**),[72] 4-(1,2,2-triphenylethenyl)benzaldehyde (**1**),[73] 1,1,2,2-tetraphenylethene (**TPE**),[74] 1,4-bis(chloromethyl)-2-(2′-ethylhexyloxy)-5-methoxybenzene[75] were synthesized according to literature.

Methods. ^{1}H, ^{13}C and ^{29}Si NMR spectra were recorded on JEOL EX400 and AL400 instruments at 400, 100 and 80 MHz respectively. Samples were analyzed in $CDCl_3$. The chemical shift values were expressed relative to Me_4Si as an internal standard in $CDCl_3$. Analytical thin layer chromatography (TLC) was performed with silica gel 60 Merck F254 plates. Column chromatography was performed with Wakogel® C-300 silica gel. High-resolution mass (HRMS) spectrometry was performed at the Technical Support Office (Department of Synthetic Chemistry and Biological Chemistry, Graduate School of Engineering, Kyoto University), and the HRMS spectra were obtained on a Thermo Fisher Scientific EXACTIVE spectrometer for Matrix Assisted Laser Desorption/Ionization (MALDI) and a Thermo Fisher Scientific EXACTIVE spectrometer for atmospheric pressure chemical ionization (APCI). UV–vis spectra were recorded on a SHIMADZU UV-3600 spectrophotometer, and samples were analyzed at room temperature. Fluorescence emission spectra were measured with a

HORIBA JOBIN YVON Fluorolog–3 spectrofluorometer and an Oxford Optistat DN for temperature control. Absolute photoluminescence quantum efficiency (Φ_{PL}) was recorded on a Hamamatsu Photonics Quantaurus-QY Plus C13534-01. Elemental analyses were performed at the Microanalytical Center of Kyoto University. Thermogravimetric analysis (TGA) was recorded on a Hitachi High-Tech Science Corporation. TA STA7200RV. Scanning electron microscopy (SEM) recorded on a JEOL JSM-6610A.

Synthesis and analytical procedures. The detailed synthetic method is reported in the Supporting Information. Figure 1 shows structures of the synthesized compounds, **TPE-POSS**, *N*-propylmethanimine-modified TPE (**TPE-Pr**), **TPE** and **MEH-PPV**. **TPE-POSS** was easily synthesized by a condensation reaction of octakis(3-aminopropyl) POSS hydrochloride (**Amino-POSS**) and 4-(1,2,2-triphenylethenyl)benzaldehyde (**1**) in 86% isolated yield. **TPE-Pr** was also prepared by the same condensation reaction of propylamine and **1** quantitatively. The luminescent π-conjugated polymer **MEH-PPV** was synthesized according to the literature.[76] We prepared two types of **MEH-PPV** with different molecular weights (M_n = 64,000 and M_w/M_n = 4.8, and M_n = 114,000 and M_w/M_n = 3.7) determined by size-exclusion chromatography with polystyrene standards with chloroform as an eluent. Both polymers had enough molecular weights to show good film formability and saturated optical properties. In addition, there were no critical differences between these polymers in the point of providing the thermally stable hybrid films exhibiting white-light emission through this study. The structures of all new compounds were confirmed by ^{1}H, ^{13}C and ^{29}Si NMR spectroscopies (Charts S1–S7), a high-resolution mass spectrometry and elemental analyses.

Preparation of hybrid films. Hybrid films were prepared by a spin-coating method (1000 rpm, 30 s) on quartz substrates (0.9 cm × 5 cm) from the chloroform solutions. The concentration of **MEH-PPV** in chloroform was fixed at 1.0 mg/300 μL. Thin films were required to evaluate proper data of optical properties without saturation.

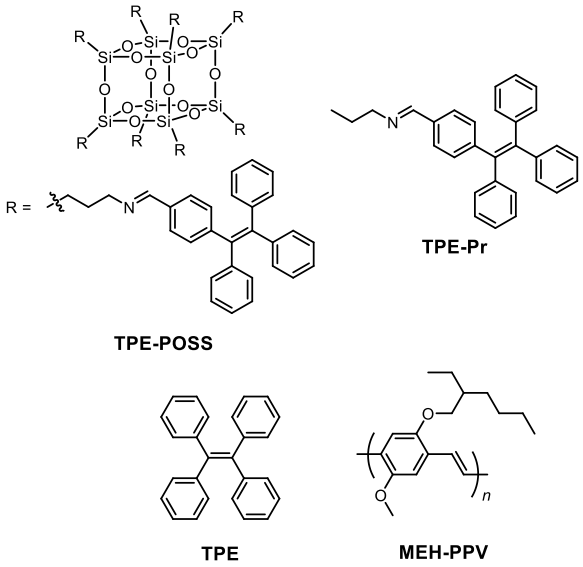

Figure 1. Structures of **TPE-POSS**, **TPE-Pr**, **TPE** and **MEH-PPV**.

Results and Discussion

The content ratios of TPE derivatives to **MEH-PPV**, which are represented as x in the abbreviation of samples (TPE derivative-x), were varied from 0 to 90 wt%. From the photos of the obtained hybrid films, both of absorption and emission colors of **TPE-POSS-x** and **TPE-Pr-x** seemed to be homogeneous (Figures 2A, B, D, E), whereas those of **TPE-x** were heterogeneous (Figures 2C, F). It is proposed that crystallinity and cohesive force of the pristine TPE were too high to hybridize with **MEH-PPV**. In contrast, homogeneous state can be realized in the presence of POSS. From scanning electron microscope (SEM) images, it was also confirmed that there were no microscale aggregates in **TPE-POSS-90** and **TPE-Pr-90**, meanwhile a phase separated pattern was observable in **TPE-90** (Figure S1A).

To obtain quantitative information from optical spectra, the spectra were normalized at the peak top of the absorption bands of **MEH-PPV**. The absorption bands of the hybrid films derived from **TPE-POSS**, **TPE-Pr**, **TPE** and **MEH-PPV** were detected at around 330, 330, 320 and 500 nm, respectively. Those peaks were also monitored in the non-hybridized pristine samples (Figure S2 and Table S1). Therefore, we selected the magnitude of absorption at 330 nm for **TPE-POSS-x** and **TPE-Pr-x**, and 320 nm for **TPE-x** to estimate the loading ratios (Figure S3 and Table S2). To obtain relative PL spectra, the relative intensity was calculated from absorbances and absolute PL quantum yields (Φ_{PL}s) obtained from original PL spectra (Figures S4 to S6 and Tables S3 to S5). The synthesis, film preparation and calculation details are described in the Supporting Information.

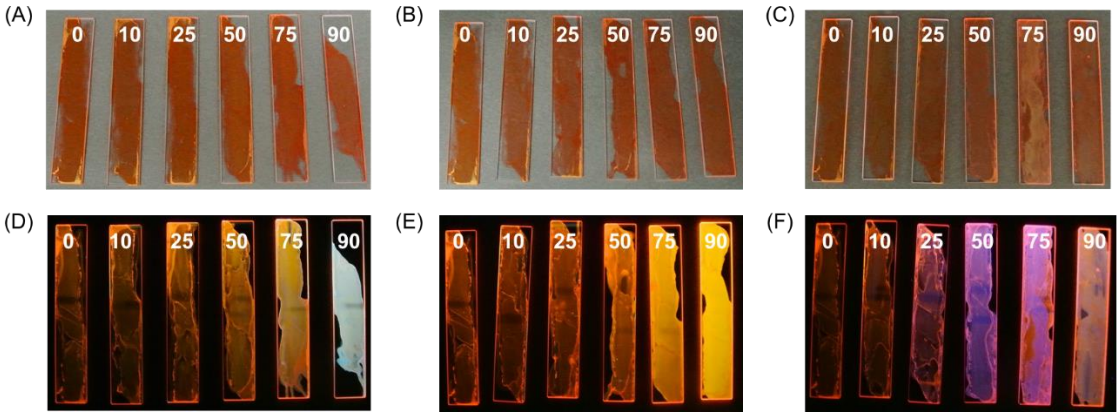

Figure 2. Photos of **TPE-POSS**, **TPE-Pr** and **TPE** hybrid films (A, B, C) under room light, (D, E, F) irradiated by UV lamp (365 nm). Inserted numbers denote content ratios (wt%) of TPE derivatives. 0 wt% means a pristine **MEH-PPV** film. Excitation light was at the wavelengths of absorption maxima. The molecular weight of using **MEH-PPV** was M_n = 64,000, M_w/M_n = 4.8.

Thermal properties

To investigate the thermal stability of the hybrids, we estimated decomposition temperature (T_d) with a thermal gravimetric analysis (TGA). The results are shown in Figure 3 and Table 1. The T_d of **TPE-POSS** (T_d = 363 °C) was much higher than those of **TPE-Pr** (T_d = 291 °C) and **TPE** (T_d = 211 °C). The extraordinary high thermal stability of **TPE-POSS** was stem from the rigid and cubic silica-based inorganic core of POSS and increase in the molecular weight.[64] The stability was inherited to the hybrid film. From the TGA profiles, pyrolysis occurred in the single step in **TPE-POSS-x** (T_d = ca. 380 °C), while **TPE-Pr-x** and **TPE-x** showed two-step decompositions. The first one (T_{d1}) and the second one (T_{d2} = ca. 400 °C) were assigned to TPE derivatives and **MEH-PPV**, respectively. As a result, T_{d1}s of the hybrid films were at around 170 to 200 °C that was critically lowered thermal stability. Those results clearly represent that the POSS-based hybridization with simple mixing in solution should be a valid strategy for obtaining thermally-stable materials, similarly to conventional hybrids prepared through sol–gel reactions.

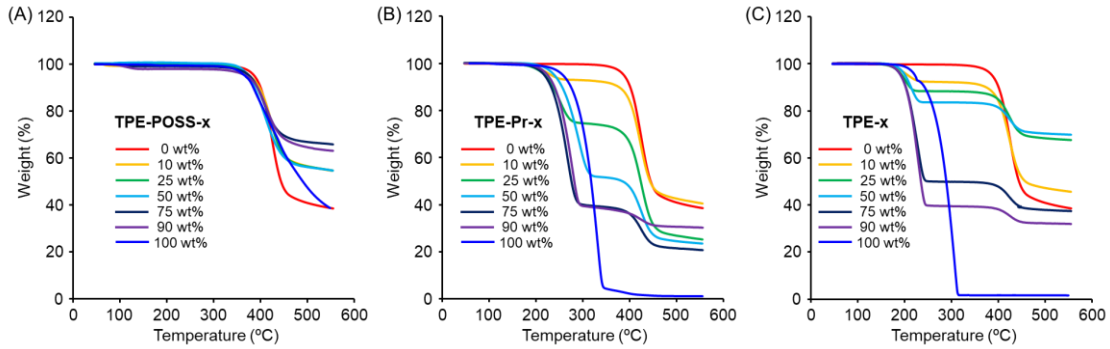

Figure 3. TGA curves of (A) **TPE-POSS-x**, (B) **TPE-Pr-x** and (C) **TPE-x** under N_2 (scan rate, 10 °C min^{-1}). 0 wt% means pristine **MEH-PPV** and 100 wt % means pristine **TPE-POSS**, **TPE-Pr** and TPE, respectively. The molecular weight of using **MEH-PPV** was M_n = 64,000, M_w/M_n = 4.8.

Table 1. Decomposition temperatures of hybrid films with **MEH-PPV** [a]

x	**TPE-POSS-x**	**TPE-Pr-x**		**TPE-x**	
(wt%)	T_d [c] (ºC)	T_{d1} [c] (ºC)	T_{d2} [d] (ºC)	T_{d1} [c] (ºC)	T_{d2} [d] (ºC)
0	397	–	397	–	397
10	390	191	395	173	396
25	384	214	398	178	396
50	372	246	399	189	398
75	377	228	400	197	397
90	381	237	399	200	399
100 [b]	363	291	–	211	–

[a] M_n = 64,000, M_w/M_n = 4.8.

[b] Pristine **TPE-POSS**, **TPE-Pr** and **TPE**.

[c] Onset temperature of the first degradation curve calculated from an extrapolation method

[d] Onset temperature of the second degradation curve calculated from an extrapolation method

Optical properties

To evaluate influence of concentrations on optical properties of the films, UV–vis absorption measurements were executed (Figures 4 and Table 2). From the spectra, the absorbance originated from **TPE-POSS**, **TPE-Pr** and **TPE** linearly increased in the hybrid films as rising their content ratios (Figure S3 and Table S2). It should be noted that significant peak broadening and shifts were hardly observed from the spectra of **TPE-POSS**-loaded hybrids, meaning that isolation states of TPE moieties should be maintained even in the presence of larger percentages of **TPE-POSS**.

Next, we measured photoluminescence (PL) spectra of the hybrid films (Figure 5 and Table 2). The relative intensity intended to be enhanced as increasing the content ratio of TPE derivatives, especially in the 75 and 90 wt% hybrid films. It is implied that degrees of **MEH-PPV** aggregates might be lowered by the TPE derivatives. This speculation can be supported by the increases in Φ_{PL}s of **MEH-PPV** by adding TPE derivatives. When irradiated with the light at 500 nm, only the **MEH-PPV** component is excited even in the presence of TPE and/or other species. Therefore, influence of the additives on the absolute PL quantum efficiency ($\Phi_{PL,500}$) of **MEH-PPV** can be evaluated. The emission enhancements were observed by adding TPE-derivatives. The $\Phi_{PL,500}$s were 9% and 12% for **TPE-POSS-75** and **TPE-POSS-90**, 11% and 19% for **TPE-Pr-75** and **TPE-Pr-90**, 12% and 12% for **TPE-75** and **TPE-90**, respectively, while the pristine **MEH-PPV** film showed lower efficiency (Φ_{PL} = 6.5%). As is often the case with conjugated polymers, the decrease in Φ_{PL} should be caused mainly by self-absorption of condensed polymer chains. In comparison to the PL spectrum of **MEH-PPV** in solution, the bathochromic shift was observed in film, strongly

suggesting that aggregation should occur in the condensed state (Figure S2D). By loading TPE derivatives, chain entanglements could be released, resulting in emission enhancement.

TPE-Pr-x exhibited the single emission band attributable to luminescence from **MEH-PPV** (Figure 5B). It is likely that FRET should efficiently proceed in the condensed state from **TPE-Pr** to the **MEH-PPV** matrix because of well overlapping between the emission spectra of TPE-derivatives and the absorption spectrum of **MEH-PPV** (Figures S2B and S2D). Estimated FRET efficiencies from the PL spectra were 100% though the all **TPE-Pr** containing hybrid films (Table S7). From the excitation spectra monitored at the peak wavelength of the emission band, contribution of the TPE absorbance area clearly supported the occurrence of energy transfer (Figure S7). In contrast, **TPE-POSS-x** (x = 75 and 90) and **TPE-x** (x = 10 to 90) showed dual emissions consisting of the emission bands of **TPE-POSS** and **TPE** with the peak around 480 nm and 440 nm, respectively, and **MEH-PPV** around 590 nm (Figures 5A and 5C). In this case, calculated FRET efficiencies from the PL spectra decreased to be 99~95% under the dual emissions (Tables S6 and S8). In particular, **TPE-POSS-90** demonstrated white emission originating from the fine combination of the dual-emission bands according to the CIE coordinate ((x, y) = (0.43, 0.40), Figure S8 and Table S9). Considering that the phase separated SEM image of **TPE-90** (Figure S1), each phase should provide intrinsic emission bands independently. As a result, dual-emission properties were obtained from **TPE-x** (x = 50, 75 and 90). In the case of POSS hybrid films, although significant inhomogeneity was hardly observed even in **TPE-POSS-90**, most of **TPE-POSS** should be far from **MEH-PPV**. Thus, the TPE

moiety can provide intrinsic emission in film.

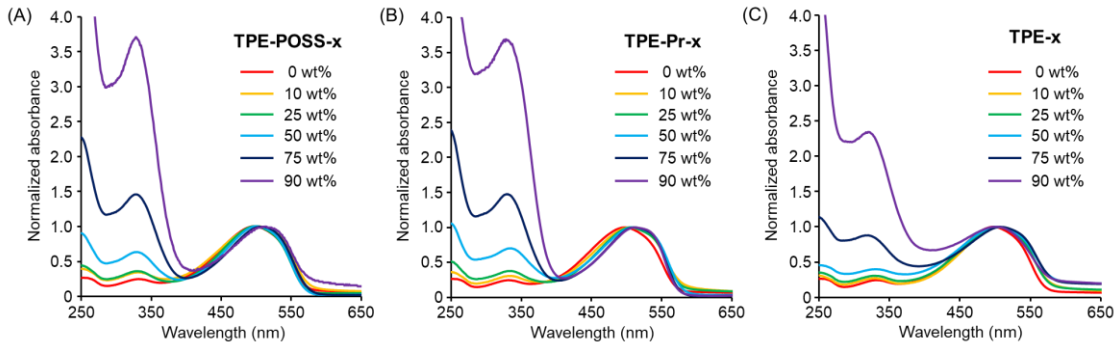

Figure 4. UV–vis absorption spectra of (A) **TPE-POSS**, (B) **TPE-Pr** and (C) **TPE** hybrid films. 0 wt% means a pristine **MEH-PPV** film. The spectra were normalized by absorption maxima of **MEH-PPV**. The molecular weight of using **MEH-PPV** was M_n = 64,000, M_w/M_n = 4.8.

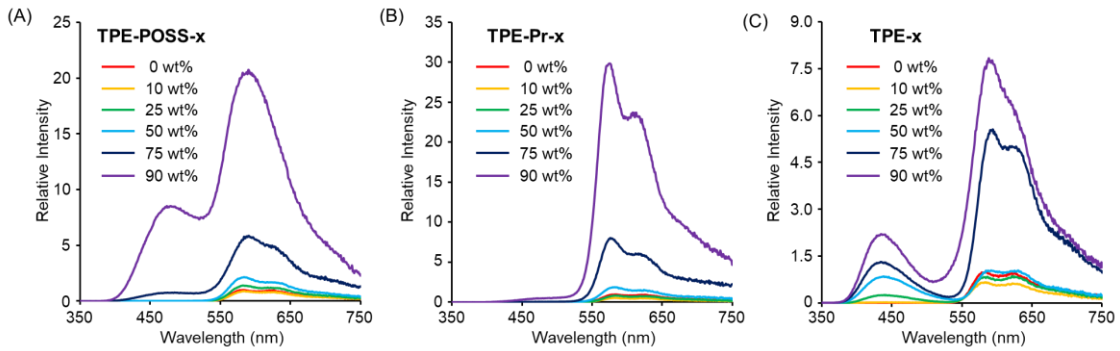

Figure 5. Relative PL spectra of (A) **TPE-POSS**, (B) **TPE-Pr** and (C) TPE hybrid films, excited at 330 nm. Inserted numbers denote content ratios of TPE derivatives. 0 wt% means a pristine **MEH-PPV** film. Excitation light was at the wavelengths of absorption maxima. The molecular weight of using **MEH-PPV** was M_n = 64,000, M_w/M_n = 4.8.

Table 2. Optical data of hybrid films with **MEH-PPV** [a]

x (wt%)	TPE-POSS-x				TPE-Pr-x				TPE-x			
	λ_{abs} (nm)	λ_{PL} (nm)[a]	$\Phi_{PL,330}$ (%)[b]	$\Phi_{PL,500}$ (%)[c]	λ_{abs} (nm)	λ_{PL} (nm)[b]	$\Phi_{PL,330}$ (%)[b]	$\Phi_{PL,500}$ (%)[c]	λ_{abs} (nm)	λ_{PL} (nm)[b]	$\Phi_{PL,330}$ (%)[b]	$\Phi_{PL,500}$ (%)[c]
0	497	583	7.3	6.5	497	583	7.3	6.5	497	583	7.3	6.5
10	330, 502	585	6.7	6.5	333, 506	582	5.2	5.2	328, 502	583	6.5	6.7
25	330, 498	582	6.9	6.6	336, 506	581	5.6	5.4	329, 502	439, 586	7.7	7.6
50	329, 501	584	7.1	7.5	336, 508	582	5.8	5.6	330, 503	438, 587	7.6	8.3
75	329, 507	485, 591	9.5	9.0	330, 511	576	10	11	320, 507	434, 594	12	12
90	330, 511	479, 590	13	12	328, 512	575	18	19	320, 501	434, 593	11	12

[a] M_n = 64,000, M_w/M_n = 4.8

[b] Excited at 330 nm.

[c] Excited at 500 nm.

To evaluate thermal enhancement to luminescent properties by the POSS-based hybridization, we monitored PL spectra with **TPE-POSS-90**, **TPE-Pr-90** and **TPE-90** by annealing at 60 °C for 12 h (Figures 6 and S9). After the heating treatments, crucial changes in emission bands were observed from the films in the absence of POSS, meanwhile the shape of the PL spectrum can be preserved in **TPE-POSS-90**, meaning that POSS can play a critical role in improving thermal robustness of luminescent properties. Regarding spectrum changes, we also detected larger intensity from the annealed **MEH-PPV** film than that of the pristine one (Figure S10). It is proposed that inhomogeneity in **TPE-90** should be enlarged by annealing (Figure S1B), followed by emission enhancement through the polymer chain rearrangement. In the case of **TPE-Pr-90**, the sharp emission band probably caused from an independent polymer chain was obtained before the treatment. It is assumed that the annealing promoted polymer aggregation, resulting in apparent bathochromic shift of absorption (Figure S9B) and emission as well as decrease in intensity. We also examined PL spectra in the much higher temperature region from 300 K to 500 K (Figures S11 and S12). The emission intensity was reduced by increasing temperature. It is because thermal motion should be activated, and excitation states are readily decayed.[39,40] The impressive point was that the two components of dual emission of **TPE-POSS-90** simultaneously decreased by elevating temperature (Figure S12A). This should be because radially integrated bulky phenyl substituents with no alkyl chain of **TPE-POSS** suppress intra- and intermolecular interactions (Figure S2A), and they can provide stable circumstances against external stimulation. Consequently, **MEH-PPV** surrounded by **TPE-POSS** is protected from morphological change and thermal quenching behavior of **MEH-PPV** followed that of **TPE-POSS**.

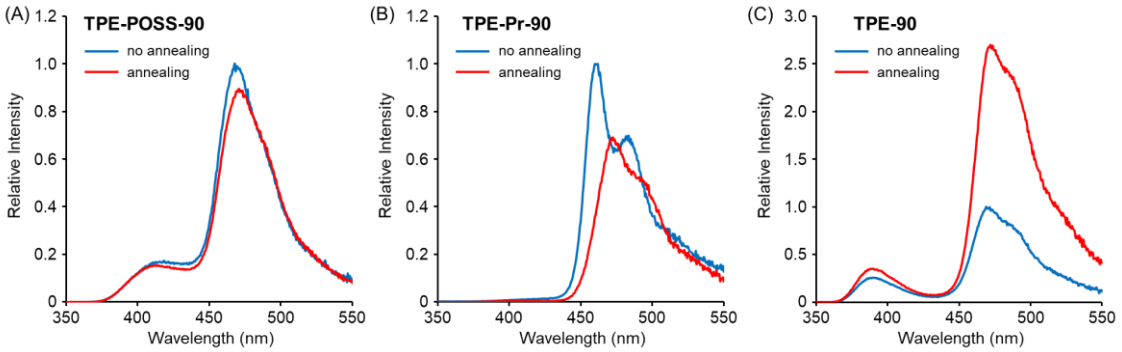

Figure 6. Relative PL spectra of (A) **TPE-POSS**, (B) **TPE-Pr** and (C) **TPE** hybrid films before and after annealing, excited at 330 nm. Annealing was carried out at 60 ºC for 12 h under vacuum condition. The molecular weight of using **MEH-PPV** was M_n = 114,000, M_w/M_n = 3.7.

Thermally stable white-light luminescent materials

Finally, we demonstrate thermal durability of while-light emission in the POSS hybrid films. In general, the color balance to exhibit white light is easily altered in the dye-mixture materials by heating because each emission property has different sensitivity toward environmental changes and is independently degraded. In contrast, both of **TPE-POSS** and **MEH-PPV** had high thermal stability and showed simultaneous degradation behaviors by heating as shown above. From these data, we presumed that the POSS-based hybrids **TPE-POSS-x** could provide white-light emission in the wide temperature ranges. Initially, by modulating the introduction ratio of **TPE-POSS** in the **MEH-PPV** matrix, color balance was tuned according to the CIE coordinates. Accordingly, almost ideal white-light emission properties were obtained from two samples, **TPE-POSS-95** ((x, y) = (0.36, 0.41)) and **TPE-POSS-98** ((x, y) = (0.37, 0.39)). We carried out the variable temperature (VT) PL measurements and monitored changes in CIE coordinates (x, y) with **TPE-POSS-95** and **TPE-POSS-98** (Figures 7 and S13). It was demonstrated that the VT PL behaviors were almost same with that of **TPE-POSS-90**. The CIE diagrams confirmed that the balance of cyan emission from **TPE-POSS** and orange emission from **MEH-PPV** almost remained at 425 K. Owing to good compatibility of POSS and conjugated polymers, not only thermal reinforcement but also good dispersion can be accomplished in the high temperature region. Therefore, the hybrid films having thermally-stable white-light emission were able to be obtained through facile mixing and painting procedures.

It was noted that the shapes of the spectra were faintly varied from 350 K and that were critically shown at over 450 K in which the CIE coordinate reached from yellow to orange region (Figures 7 and S12). The reason might be photodegradation of PL

intensity induced by a photocyclization of the TPE moiety.[77] From the evaluation of repeatability of the VT PL spectra of **TPE-POSS-90**, the PL intensity was recovered by a colling process although thermal degradation was partially observed in every cycle (Figure S14). This means that the reduction of PL intensity by heating was mainly attributed to thermal quenching. By monitoring the PL intensity at 400 K for 100 min (Figure S15), it was revealed that gradual thermal degradation of the PL intensity occurred at high temperature. However, the degradation speed became slow after 50 min heating time, especially in the emission from **MEH-PPV** at 580 nm (Figure S15C). Continuous degradation of the emission from **TPE-POSS** at 480 nm over 50 min heating time might be caused by the photocyclization accelerated by heating. As a result, the while-light emissive film changed the color into orange after heating especially over 450 K. The photo-masked area was not influenced by the degradation and still showed white-light emission after heating at 400 K over 100 min.

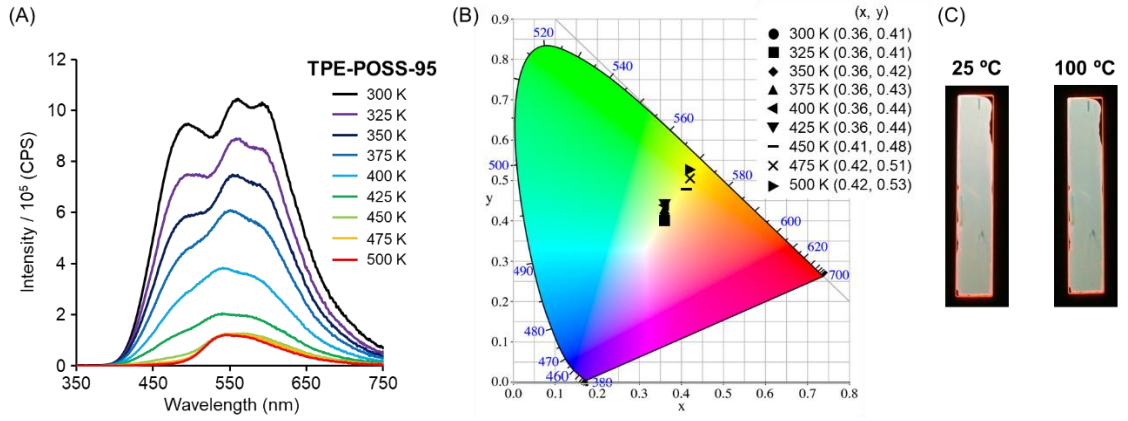

Figure 7. (A) Variable temperature (VT) PL spectra, (B) CIE diagram and (C) photos under heating (excited by UV lamp (365 nm)) of **TPE-POSS-95**. The film samples were prepared by a spin-coating method from chloroform solutions on quartz substrates. The molecular weight of using **MEH-PPV** was M_n = 114,000, M_w/M_n = 3.7.

Conclusion

We demonstrate here new advantageous optical property, thermally stable dual emission. We prepared hybrid films through the facile mixing procedure in solution composed of TPE derivatives and **MEH-PPV**. By connecting with POSS, compatibility of TPE to the conjugated polymer can be greatly improved, and homogeneous hybrid films were obtained. All POSS-based hybrids showed extremely high thermal stability toward molecular rearrangement by annealing as well as pyrolysis. Therefore, enhanced emission efficiencies by the suppression of polymer chain aggregation can be maintained by heating. It should be emphasized that the hybrid films containing **TPE-POSS** showed a thermally stable dual-emission property, and white-light luminescence was also achieved by modulating mixing ratios. In particular, owing to thermally stable well dispersion of **TPE-POSS**, dual-emission properties were also preserved even in the high temperature region (425 K). Finally, white-light luminescent materials with thermal durability were obtained. Hybridization with the POSS is promised to be a simple and versatile method to create color selective and thermally stable light-emitting materials.

Associated Content

Supporting Information

Synthetic procedures and characterization. SEM observations (Figure S1). Optical data of compounds in solution and film states (Figure S2 and Table S1). Liner relationships of content ratios and absorbances (Figure S3 and Table S2). The detail method for estimation of the relative PL spectra (Figures S4–S6 and Tables S3–S5). FRET efficiency (Tables S6–S8). Excitation spectra (Figure S7). CIE diagrams (Figure S8 and Table S6). UV–vis absorption spectra before and after annealing (Figure S9). UV–vis absorption and relative PL spectra of **MEH-PPV** before and after annealing (Figure S10). Variable temperature (VT) PL spectra of hybrid materials and **MEH-PPV** (Figure S11). Analysis of VT PL spectra of hybrid materials and **MEH-PPV** (Figure S12). VT PL spectra of **TPE-POSS-98** (Figure S13). Repeatability of VT PL spectra of **TPE-POSS-90** (Figure S14). Thermal degradation PL spectra of **TPE-POSS-90** at 400 K (Figure S15)

Acknowledgement

This work was partially supported by the Nakanishi Scholarship Foundation (for M.G.), a Grant-in-Aid for Scientific Research (A) (JP 17H01220) and a Grant-in-Aid for Scientific Research on Innovative Areas “New Polymeric Materials Based on Element-Blocks (No.2401)” (JP P24102013).

References

(1) Fresta, E.; Costa, R. D. Advances and Challenges in White Light-Emitting Electrochemical Cells. *Adv. Funct. Mater.* **2020**, *30*, 1908176.

(2) Kundu, S.; Sk, B.; Pallavi, P.; Giri, A.; Patra, A. Molecular Engineering Approaches Towards All‐Organic White Light Emitting Materials. *Chem. Eur. J.* **2020**, 26, 5557−5582.

(3) Mukherjee, S.; Thilagar, P. Organic white-light emitting materials. *Dyes Pigments* **2014**, *110*, 2−27.

(4) Chen, Z.; Ho, C.-L.; Wang, L.; Wong, W.-Y. Single-Molecular White-Light Emitters and Their Potential WOLED Applications. *Adv. Mater.* **2020**, *32*, 1903269.

(5) Kubo, Y.; Nishiyabu, R. White-light emissive materials based on dynamic polymerization in supramolecular chemistry. *Polymer* **2017**, 128, 257−275.

(6) Pallavi, P.; Sk, B.; Ahir, P.; Patra, A. Tuning the Förster Resonance Energy Transfer through a Self-Assembly Approach for Efficient White-Light Emission in an Aqueous Medium. *Chem. Eur. J.* **2018**, *24*, 1151−1158.

(7) Zhang, X.; Görl, D.; Würthner, F. White-light emitting dye micelles in aqueous solution. *Chem. Commun.* **2013**, *49*, 8178−8180.

(8) Wang, R.; Peng, J.; Qiu, F.; Yang, Y. Enhanced white-light emission from multiple fluorophores encapsulated in a single layer of diblock copolymer micelles. *Chem. Commun.* **2011**, *47*, 2787−2789.

(9) Bälter, M.; Li, S.; Morimoto, M.; Tang, S.; Hernando, J.; Guirado, G.; Irie, M.; Raymo, F. M.; Andréasson, J. Emission color tuning and white-light generation based on photochromic control of energy transfer reactions in polymer micelles.

Chem. Sci. **2016**, *7*, 5867−5871.

(10) Zhang, X.; Rehm, S.; Safont-Sempere, M. M.; Würthner, F. Vesicular perylene dye nanocapsules as supramolecular fluorescent pH sensor systems. *Nat. Chem.* **2009**, *1*, 623−629.

(11) Huang, J.; Yu, Y.; Wang, L.; Wang, X.; Gu, Z.; Zhang, S. Tetraphenylethylene-Induced Cross-Linked Vesicles with Tunable Luminescence and Controllable Stability. *ACS Appl. Mater. Interfaces* **2017**, *9*, 29030−29037.

(12) Xing, P.; Zhao, Z.; Hao, A.; Zhao, Y. Tailoring luminescence color conversion via affinitive co-assembly of glutamates appended with pyrene and naphthalene dicarboximide units. *Chem. Commun.* **2016**, *52*, 1246−1249.

(13) Feng, H.-T.; Zheng, X.; Gu, X.; Chen, M.; Lam, J. W. Y.; Huang, X.; Tang, B. Z. White-Light Emission of a Binary Light-Harvesting Platform Based on an Amphiphilic Organic Cage. *Chem. Mater.* **2018**, *30*, 1285−1290.

(14) Ni, X.-L.; Chen, S.; Yang, Y.; Tao, Z. Facile Cucurbit[8]uril-Based Supramolecular Approach To Fabricate Tunable Luminescent Materials in Aqueous Solution. *J. Am. Chem. Soc.* **2016**, *138*, 6177−6183.

(15) Ono, T.; Hisaeda, Y. Flexible-color tuning and white-light emission in three-, four-, and five-component host/guest co-crystals by charge-transfer emissions as well as effective energy transfers. *J. Mater. Chem. C* **2019**, *7*, 2829−2842.

(16) Jin, W.-H.; Lu, H.-H.; Zhang, Q.; Qu, D.-H. A dual-mode orthogonally tunable fluorescent system covering the whole white light region. *Mater. Chem. Front.* **2020**, *4*, 532−536.

(17) Zhang, Z.; Li, Y.; Geng, L.; Feng, G.; Ren, J.; Yu, X. Healable, Phase-Selective, and White-Light-Emitting Titania Based Hybrid Lanthanide-Doped Metallogels.

Inorg. Chem. **2020**, *59*, 3974−3982.

(18) Podder, D.; Nandi, S. K.; Sasmal, S.; Haldar, D. Synergistic Tricolor Emission-Based White Light from Supramolecular Organic–Inorganic Hybrid Gel. *Langmuir* **2019**, 35, 6453−6459.

(19) Cao, X.; Lan, H.; Li, Z.; Mao, Y.; Chen, L.; Wu, Y.; Yi, T. White light emission from a two-component hybrid gel via an energy transfer process. *Phys. Chem. Chem. Phys.* **2015**, 17, 32297−32303.

(20) Bairi, P.; Roy, B.; Chakraborty, P.; Nandi, A. K. Co-assembled White-Light-Emitting Hydrogel of Melamine. *ACS Appl. Mater. Interfaces* **2013**, *5*, 5478−5485.

(21) Vijayakumar, C.; Praveen, V. K.; Ajayaghosh, A. RGB Emission through Controlled Donor Self-Assembly and Modulation of Excitation Energy Transfer: A Novel Strategy to White-Light-Emitting Organogels. *Adv. Mater.* **2009**, *21*, 2059−2063.

(22) Liu, X.-Y.; Xing, K.; Li, Y.; Tsung, C.-K.; Li, J. Three Models To Encapsulate Multicomponent Dyes into Nanocrystal Pores: A New Strategy for Generating High-Quality White Light. *J. Am. Chem. Soc.* **2019**, *141*, 14807−14813.

(23) Wang, Z.; Zhu, C.-Y.; Mo, J.-T.; Fu, P.-Y.; Zhao, Y.-W.; Yin, S.-Y.; Jiang, J.-J.; Pan, M.; Su, C.-Y. White-Light Emission from Dual-Way Photon Energy Conversion in a Dye-Encapsulated Metal–Organic Framework. *Angew. Chem. Int. Ed.* **2019**, *58*, 9752−9757.

(24) Xia, Y.-P.; Wang, C.-X.; An, L.-C.; Zhang, D.-S.; Hu, T.-L.; Xu, J.; Chang, Z.; Bu, X.-H. Utilizing an effective framework to dye energy transfer in a carbazole-based metal–organic framework for high performance white light

emission tuning. *Inorg. Chem. Front.* **2018**, *5*, 2868−2874.

(25) Xie, W.; Zhang, S.-R.; Du, D.-Y.; Qin, J.-S.; Bao, S.-J.; Li, J.; Su, Z.-M.; He, W.-W.; Fu, Q.; Lan, Y.-Q. Stable Luminescent Metal–Organic Frameworks as Dual-Functional Materials To Encapsulate Ln3+ Ions for White-Light Emission and To Detect Nitroaromatic Explosives. *Inorg. Chem.* **2015**, *54*, 3290−3296.

(26) He, H.; Sun, F.; Borjigin, T.; Zhao, N.; Zhu, G. Tunable colors and white-light emission based on a microporous luminescent Zn(ii)-MOF. *Dalton Trans.* **2014**, *43*, 3716−3721.

(27) Sun, C.-Y.; Wang, X.-L.; Zhang, X.; Qin, C.; Li, P.; Su, Z.-M.; Zhu, D.-X.; Shan, G.-G.; Shao, K.-Z.; Wu, H.; Li, J. Efficient and tunable white-light emission of metal–organic frameworks by iridium-complex encapsulation. *Nat. Commun.* **2013**, *4*, 2717.

(28) Newsome, W.; Ayad, S.; Cordova, J.; Reinheimer, E. W.; Campiglia, A. D.; Harper, J. K.; Hanson, K.; Uribe-Romo, F. J. Solid State Multicolor Emission in Substitutional Solid Solutions of Metal–Organic Frameworks. *J. Am. Chem. Soc.* **2019**, *141*, 11298−11303.

(29) Kumar, S.; Hisamatsu, Y.; Tamaki, Y.; Ishitani, O.; Aoki, S. Design and Synthesis of Heteroleptic Cyclometalated Iridium(III) Complexes Containing Quinoline-Type Ligands that Exhibit Dual Phosphorescence. *Inorg. Chem.* **2016**, *55*, 3829−3843.

(30) Han, M.; Tian, Y.; Yuan, Z.; Zhu, L.; Ma, B. A Phosphorescent Molecular “Butterfly” that undergoes a Photoinduced Structural Change allowing Temperature Sensing and White Emission. *Angew. Chem. Int. Ed.* **2014**, *53*, 10908−10912.

(31) Karpiuk, J.; Karolak, E.; Nowacki, J. Tuneable white fluorescence from intramolecular exciplexes. *Phys. Chem. Chem. Phys.* **2010**, *12*, 8804−8809.

(32) Jin, X.-H.; Chen, C.; Ren, C.-X.; Cai, L.-X.; Zhang, J. Bright white-light emission from a novel donor–acceptor organic molecule in the solid state via intermolecular charge transfer. *Chem. Commun.* **2014**, *50*, 15878−15881.

(33) Lee, J.; Kim, B.; Kwon, J. E.; Kim, J.; Yokoyama, D.; Suzuki, K.; Nishimura, H.; Wakamiya, A.; Park, S. Y.; Park, J. Excimer formation in organic emitter films associated with a molecular orientation promoted by steric hindrance. *Chem. Commun.* **2014**, *50*, 14145−14148.

(34) Zhou, C.; Zhang, S.; Gao, Y.; Liu, H.; Shan, T.; Liang, X.; Yang, B.; Ma, Y. Ternary Emission of Fluorescence and Dual Phosphorescence at Room Temperature: A Single-Molecule White Light Emitter Based on Pure Organic Aza-Aromatic Material. *Adv. Funct. Mater.* **2018**, *28*, 1802407.

(35) He, Z.; Zhao, W.; Lam, J. W. Y.; Peng, Q.; Ma, H.; Liang, G.; Shuai, Z.; Tang, B. Z. White light emission from a single organic molecule with dual phosphorescence at room temperature. *Nat. Commun.* **2017**, *8*, 416.

(36) Pati, A. K.; Jana, R.; Gharpure, S. J.; Mishra, A. K. Photophysics of Diphenylbutadiynes in Water, Acetonitrile–Water, and Acetonitrile Solvent Systems: Application to Single Component White Light Emission. *J. Phys. Chem. A* **2016**, *120*, 5826−5837.

(37) Tu, D.; Leong, P.; Guo, S.; Yan, H.; Lu, C.; Zhao, Q. Highly Emissive Organic Single-Molecule White Emitters by Engineering o-Carborane-Based Luminophores. *Angew. Chem. Int. Ed.* **2017**, *56*, 11370−11374.

(38) Tominaga, M.; Naito, H.; Morisaki, Y.; Chujo, Y. Colour-tunable

aggregation-induced emission of trifunctional o-carborane dyes. *New J. Chem.* **2014**, *38*, 5686−5690.

(39) Younis, O.; El-Katori, E. E.; Hassanien, R.; Abousalem, A. S.; Tsutsumi, O. Luminescent coatings: White-color luminescence from a simple and single chromophore with high anticorrosion efficiency. *Dyes Pigments* **2020**, *175*, 108146.

(40) Qiao, J.; Zhao, J.; Liu, Q.; Xia, Z. Recent advances in solid-state LED phosphors with thermally stable luminescence. *J. Rare Earths* **2019**, *37*, 565−572.

(41) Lee, J. U.; Jung, J. W.; Jo, J. W.; Jo, W. H. Degradation and stability of polymer-based solar cells. *J. Mater. Chem.* **2012**, *22*, 24265−24283.

(42) Kajiwara, Y.; Nagai, A.; Tanaka, K.; Chujo, Y. Efficient simultaneous emission from RGB-emitting organoboron dyes incorporated into organic–inorganic hybrids and preparation of white light-emitting materials. *J. Mater. Chem. C* **2013**, *1*, 4437−4444.

(43) Cordes, D. B.; Lickiss, P. D.; Rataboul, F. Recent Developments in the Chemistry of Cubic Polyhedral Oligosilsesquioxanes. *Chem. Rev.* **2010**, *110*, 2081−2173.

(44) Schwab, J. J.; Lichtenhan, J. D. Polyhedral oligomeric silsesquioxane(POSS)-based polymers. *Appl. Organometal. Chem.* **1998**, *12*, 707−713.

(45) Wang, F. K.; Lu, X.; He, C. Some recent developments of polyhedral oligomeric silsesquioxane (POSS)-based polymeric materials. *J. Mater. Chem.* **2011**, *21*, 2775−2782.

(46) Tanaka, K.; Chujo, Y. Modulation of the solid-state luminescent properties of

conjugated polymers by changing the connecting points of flexible boron element blocks. *Polym. J.* **2020**, *52*, 555−566.

(47) Gon, M.; Tanaka, K.; Chujo, Y. Recent progress in the development of advanced element-block materials. *Polym. J.* **2018**, *50*, 109−126.

(48) Gon, M.; Tanaka, K.; Chujo, Y. Creative Synthesis of Organic–Inorganic Molecular Hybrid Materials. *Bull. Chem. Soc. Jpn.* **2017**, *90*, 463−474.

(49) Chujo, Y.; Tanaka, K. New Polymeric Materials Based on Element-Blocks. *Bull. Chem. Soc. Jpn.* **2015**, *88*, 633−643.

(50) Ueda, K.; Kakuta, T.; Tanaka, K.; Chujo, Y. High Refractive-Index Hybrids Consisting of Water-Soluble Matrices with Bipyridine-Modified Polyhedral Oligomeric Silsesquioxane and Lanthanoid Cations. *Polymers* **2020**, *12*, 1560.

(51) Morisue, M.; Kusukawa, T.; Watase, S. Dipyrrin Complexes of Borasiloxane Silanols with Adaptive Hydrogen-Bonded Conformations in the Crystal and in Solution States. *Eur. J. Inorg. Chem.* **2020**, 1885−1893.

(52) Ueda, K.; Tanaka, K.; Chujo, Y. Molecular fillers for increasing the refractive index of polystyrene hybrids by chain assembly at polyhedral oligomeric silsesquioxane. *Polym. J.* **2020**, *52*, 523−528.

(53) Dang, H.; Li, Y.; Zou, H.; Liu, S. Tunable white-light emission hybrids based on lanthanide complex functionalized poly (ionic liquid): Assembly and chemical sensing. *Dyes Pigments* **2020**, *172*, 107804.

(54) Matsumura, Y.; Nishiyama, H.; Inagi, S.; Tomita, I. Synthesis of π-conjugated polymer containing both thiophene and phosphole sulfide in the main chain by simultaneous post-element transformation of organotitanium polymer. *J. Polym. Sci. Part A: Polym. Chem.* **2019**, *57*, 2519−2525.

(55) Katoh, R.; Imoto, H.; Naka, K. One-pot strategy for synthesis of open-cage silsesquioxane monomers. *Polym. Chem.* **2019**, *10*, 2223−2229.

(56) Chatterjee, S.; Ooya, T. Hydrophobic Nature of Methacrylate-POSS in Combination with 2-(Methacryloyloxy)ethyl Phosphorylcholine for Enhanced Solubility and Controlled Release of Paclitaxel. *Langmuir* **2019**, *35*, 1404−1412.

(57) Saito, S.; Wada, H.; Shimojima, A.; Kuroda, K. Synthesis of Zeolitic Macrocycles Using Site-Selective Condensation of Regioselectively Difunctionalized Cubic Siloxanes. *Inorg. Chem.* **2018**, *57*, 14686−14691.

(58) Hayami, R.; Wada, K.; Miyase, Y.; Sagawa, T.; Tsukada, S.; Yamamoto, K.; Gunji, T. Properties and surface morphologies of organic–inorganic hybrid thin films containing titanium phosphonate clusters. *Polym. J.* **2018**, *50*, 1169−1177.

(59) Ariga, K.; Leong, D. T.; Mori, T. Nanoarchitectonics for Hybrid and Related Materials for Bio-Oriented Applications. *Adv. Funct. Mater.* **2018**, *28*, 1702905.

(60) Nakamura, R.; Narikiyo, H.; Gon, M.; Tanaka, K.; Chujo, Y. An optical sensor for discriminating the chemical compositions and sizes of plastic particles in water based on water-soluble networks consisting of polyhedral oligomeric silsesquioxane presenting dual-color luminescence. *Mater. Chem. Front.* **2019**, *3*, 2690−2695.

(61) Kato, K.; Gon, M.; Tanaka, K.; Chujo, Y. Stretchable Conductive Hybrid Films Consisting of Cubic Silsesquioxane-capped Polyurethane and Poly(3-hexylthiophene). *Polymers* **2019**, *11*, 1195.

(62) Nakamura, R.; Narikiyo, H.; Gon, M.; Tanaka, K.; Chujo, Y. Oxygen-Resistant Electrochemiluminescence System with Polyhedral Oligomeric Silsesquioxane. *Polymers* **2019**, *11*, 1170.

(63) Gon, M.; Kato, K.; Tanaka, K.; Chujo, Y. Elastic and mechanofluorochromic hybrid films with POSS-capped polyurethane and polyfluorene. *Mater. Chem. Front.* **2019**, *3*, 1174−1180.

(64) Guan, J.; Tomobe, K.; Madu, I.; Goodson, T.; Makhal, K.; Trinh, M. T.; Rand, S. C.; Yodsin, N.; Jungsuttiwong, S.; Laine, R. M. Photophysical Properties of Partially Functionalized Phenylsilsesquioxane: $[RSiO_{1.5}]_7[Me/nPrSiO_{1.5}]$ and $[RSiO_{1.5}]_7[O_{0.5}SiMe_3]_3$ (R = 4-Me/4-CN-Stilbene). Cage-Centered Magnetic Fields Form under Intense Laser Light. *Macromolecules* **2019**, *52*, 4008−4019.

(65) Gon, M.; Sato, K.; Tanaka, K.; Chujo, Y. Controllable intramolecular interaction of 3D arranged π-conjugated luminophores based on a POSS scaffold, leading to highly thermally-stable and emissive materials. *RSC Adv.* **2016**, *6*, 78652−78660.

(66) Gon, M.; Sato, K.; Kato, K.; Tanaka, K.; Chujo, Y. Preparation of bright-emissive hybrid materials based on light-harvesting POSS having radially integrated luminophores and commercial π-conjugated polymers. *Mater. Chem. Front.* **2019**, *3*, 314−320.

(67) Ueda, K.; Tanaka, K.; Chujo, Y. Remarkably high miscibility of octa-substituted POSS with commodity conjugated polymers and molecular fillers for the improvement of homogeneities of polymer matrices. *Polym. J.* **2016**, *48*, 1133−1139.

(68) Sapsford, K. E.; Berti, L.; Medintz, I. L. Materials for Fluorescence Resonance Energy Transfer Analysis: Beyond Traditional Donor–Acceptor Combinations. *Angew. Chem. Int. Ed.* **2006**, *45*, 4562−4589.

(69) Gustafsson, G.; Cao, Y.; Treacy, G. M.; Klavetter, F.; Colaneri, N.; Heeger, A. J. Flexible light-emitting diodes made from soluble conducting polymers. *Nature*

1992, *357*, 477−479.

(70) Mei, J.; Leung, N. L. C.; Kwok, R. T. K.; Lam, J. W. Y.; Tang, B. Z. Aggregation-Induced Emission: Together We Shine, United We Soar!. *Chem. Rev.* **2015**, *115*, 11718−11940.

(71) Zhao, Z.; Lam, J. W. Y.; Tang, B. Z. Tetraphenylethene: a versatile AIE building block for the construction of efficient luminescent materials for organic light-emitting diodes. *J. Mater. Chem.* **2012**, *22*, 23726−23740.

(72) Tanaka, K.; Inafuku, K.; Adachi, S.; Chujo, Y. Tuning of Properties of POSS-Condensed Water-Soluble Network Polymers by Modulating the Cross-Linking Ratio between POSS. *Macromolecules* **2009**, *42*, 3489–3492.

(73) Chua, M. H.; Ni, Y.; Garai, M.; Zheng, B.; Huang, K.-W.; Xu, Q.-H.; Xu, J.; Wu, J. Towards meso-Ester BODIPYs with Aggregation-Induced Emission Properties: The Effect of Substitution Positions. *Chem. -Asian J.* **2015**, *10*, 1631–1634.

(74) Nunes, C. M.; Steffens, D.; Monteiro, A. L. Synthesis of Tri- and Tetrasubstituted Olefins by Palladium Cross-Coupling Reaction. *Synlett* **2007**, 0103–0106.

(75) Ravnsbæk, J. B.; Swager, T. M. Mechanochemical Synthesis of Poly(phenylene vinylenes). *ACS Macro Lett.* **2014**, *3*, 305–309.

(76) Lin, K.-F.; Fan, Y.-L.; Chow, H.-L. Origin of the methylene bonds in poly[2-methoxy-5-(2′-ethyl-hexyloxy)-1,4-phenylenevinylene] prepared according to Gilch's method: novel applications. *Polym. Int.* **2006**, *55*, 938−944.

(77) Liu, S.; Cheng, Y.; Li, Y.; Chen, M.; Lam, J. W. Y.; Tang, B. Z. Manipulating Solid-State Intramolecular Motion toward Controlled Fluorescence Patterns.

ACS Nano **2020**, *14*, 2090−2098.

Supporting Information

Paintable Hybrids with Thermally Stable Dual Emission Composed of Tetraphenylethene-Integrated POSS and MEH-PPV for Heat-Resistant White-Light Luminophores

Masayuki Gon, Satoru Saotome, Kazuo Tanaka* and Yoshiki Chujo

Department of Polymer Chemistry, Graduate School of Engineering, Kyoto University Katsura, Nishikyo-ku, Kyoto 615-8510, Japan

E-mail: tanaka@poly.synchem.kyoto-u.ac.jp

Contents page

Synthetic procedures and characterization S–3

Synthesis of **TPE-POSS** S–3

Synthesis of **TPE-Pr** S–6

Synthesis of **MEH-PPV** S–8

SEM observations S–10

Optical data of compounds in solution and film states S–11

Liner relationships of content ratios and absorbances S–12

The detail method for estimation of the relative PL spectra S–13

FRET efficiency S–16

Excitation spectra S–17

CIE diagrams S–18

UV–vis absorption spectra before and after annealing S–19

Variable temperature (VT) PL spectra of hybrid materials and **MEH-PPV** S–20

Analysis of VT PL spectra of hybrid materials and **MEH-PPV** S–21

VT PL spectra of **TPE-POSS-98** S–22

Repeatability of VT PL spectra of **TPE-POSS-90** S–23

Thermal degradation PL spectra of **TPE-POSS-90** at 400 K S–24

Synthetic Procedures and Characterization

Synthesis of TPE-POSS

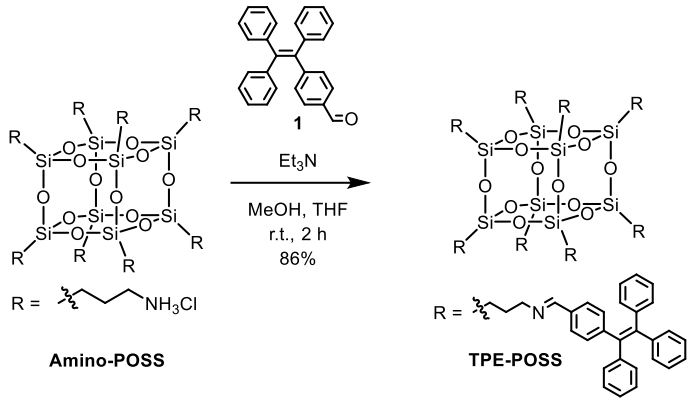

Amino-POSS (100.0 mg, 0.085 mmol) was placed in a round-bottom flask equipped with a magnetic stirring bar. MeOH (10 mL) and Et_3N (237 μL, 1.71 mmol) were added to the flask. 4-(1,2,2-triphenylethenyl)benzaldehyde (**1**) (0.426 M in THF, 2.0 mL, 0.852 mmol) was added dropwise to this stirred colorless solution. After the mixture was stirred at room temperature for 2 h, the white precipitate was washed with MeOH. The residue was purified by reprecipitation with acetone (good solvent) and −78 °C MeOH (poor solvent) to afford **TPE-POSS** (261 mg, 0.072 mmol, 86% yield) as a white solid.

^{1}H NMR ($CDCl_3$, 400 MHz) δ 8.10 (s, 8H), 7.41 (d, J = 8.1 Hz, 16H), 7.09–6.98 (m, 136H), 3.50 (t, J = 6.6 Hz, 16H), 1.75 (m, 16H), 0.64 (t, J = 7.8 Hz, 16H) ppm; ^{13}C NMR ($CDCl_3$, 100 MHz) δ 160.8, 146.2, 143.5, 143.4, 143.4, 141.7, 140.4, 134.3, 131.6, 131.3, 131.3, 131.3, 127.8, 127.7, 127.6, 127.5, 126.7, 126.6, 126.5, 64.1, 24.3, 9.7 ppm; ^{29}Si NMR ($CDCl_3$, 80 MHz) δ −66.7 (s) ppm. HRMS (MALDI) calcd. for $C_{240}H_{209}N_8O_{12}Si_8$ $[M+H]^+$: 3618.4139, found: 3618.4053. Elemental analysis calcd. for $C_{240}H_{208}N_8O_{12}Si_8$: C 79.61 H 5.79 N 3.09, found: C 78.77 H 5.73 N 3.04.

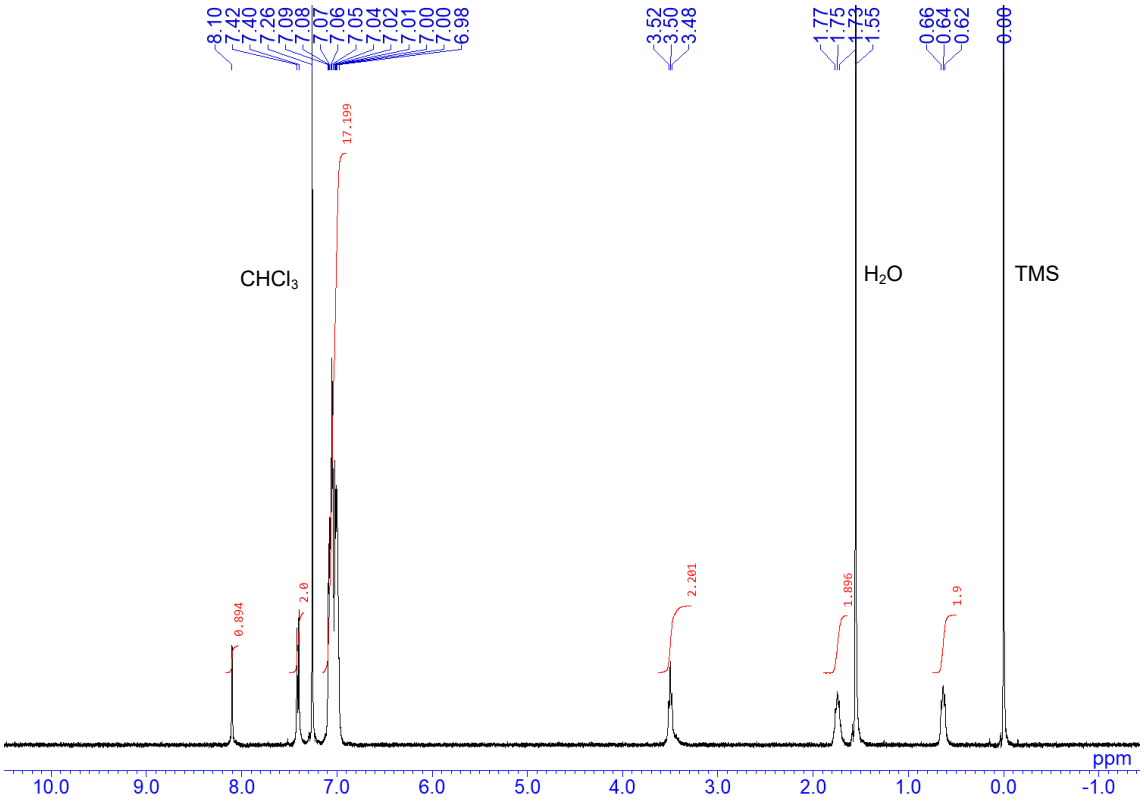

Chart S1. ^{1}H NMR spectrum of **TPE-POSS** in $CDCl_3$.

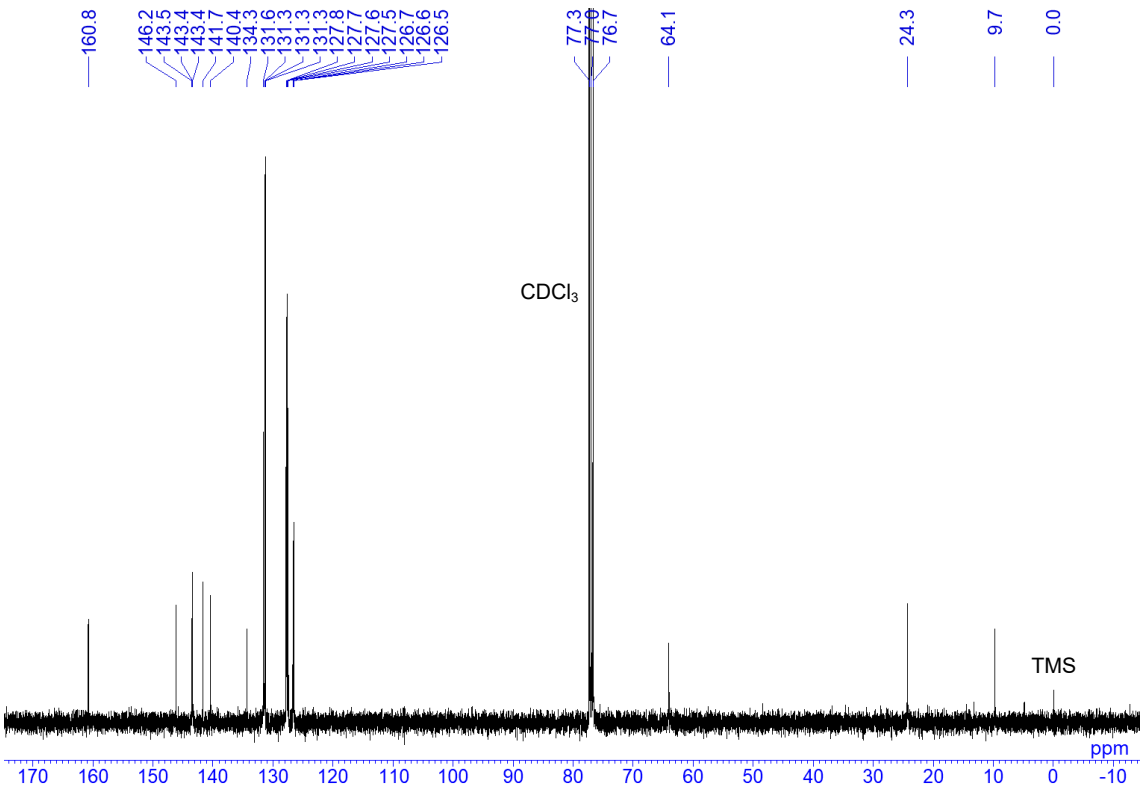

Chart S2. ^{13}C NMR spectrum of **TPE-POSS** in $CDCl_3$.

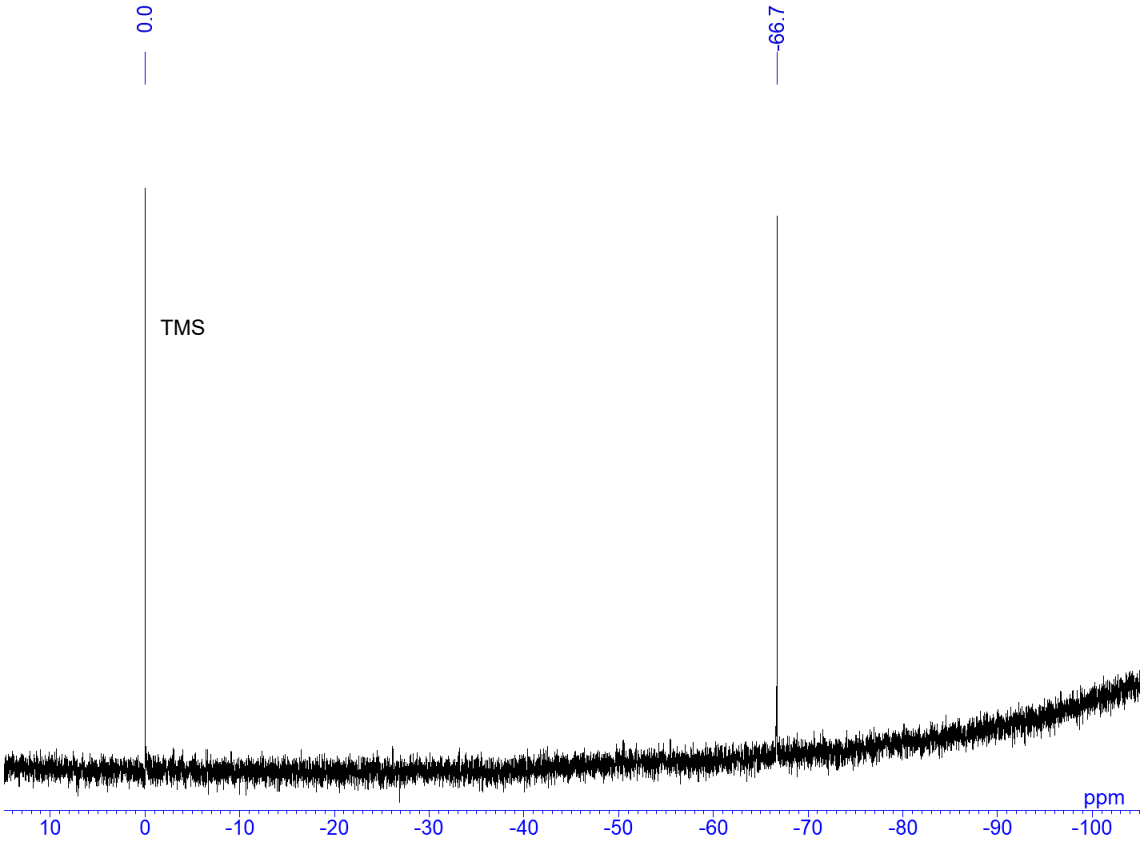

Chart S3. ^{29}Si NMR spectrum of **TPE-POSS** in $CDCl_3$.

Synthesis of TPE-Pr

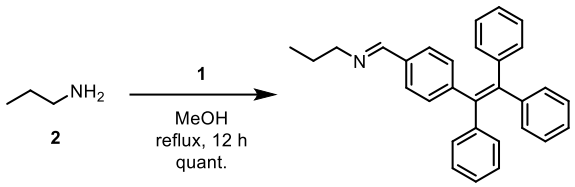

TPE-Pr

1 (100 mg, 0.277 mmol) was placed in a round-bottom flask equipped with a magnetic stirring bar. MeOH (17.0 mL) was added to the flask and the solution was heated to 70 °C. Propylamine (**2**) (22.8 μL, 0.277 mmol) was added to this stirred colorless solution. After the mixture was stirred at a reflux temperature for 12 h, the solvent was removed with a rotary evaporator. The viscous oil was dissolved in benzene, freeze drying was carried out to afford **TPE-Pr** (111 mg, 0.277 mmol, quantitative) as a white solid.

^{1}H NMR ($CDCl_3$, 400 MHz) δ 8.17 (s, 1H), 7.46 (dd, J = 6.6, 1.7 Hz, 2H), 7.11–7.00 (m, 17H), 3.53 (td, J = 7.1, 1.2 Hz, 2H), 1.69 (qt, J = 7.1, 7.1 Hz, 2H), 0.94 (t, J = 7.3 Hz, 3H) ppm; ^{13}C NMR ($CDCl_3$, 100 MHz) δ 160.7, 146.2, 143.5, 143.4, 143.4, 141.7, 140.4, 134.3, 131.6, 131.3, 131.3, 131.3, 127.8, 127.7, 127.6, 127.4, 126.6, 126.6, 126.5, 63.6, 24.1, 11.9 ppm. HRMS (APCI) calcd. for $C_{30}H_{28}N$ $[M+H]^+$: 402.2216, found: 402.2223. Elemental analysis calcd. for $C_{30}H_{27}N$: C 89.73 H 6.78 N 3.49, found: C 89.60 H 6.78 N 3.26.

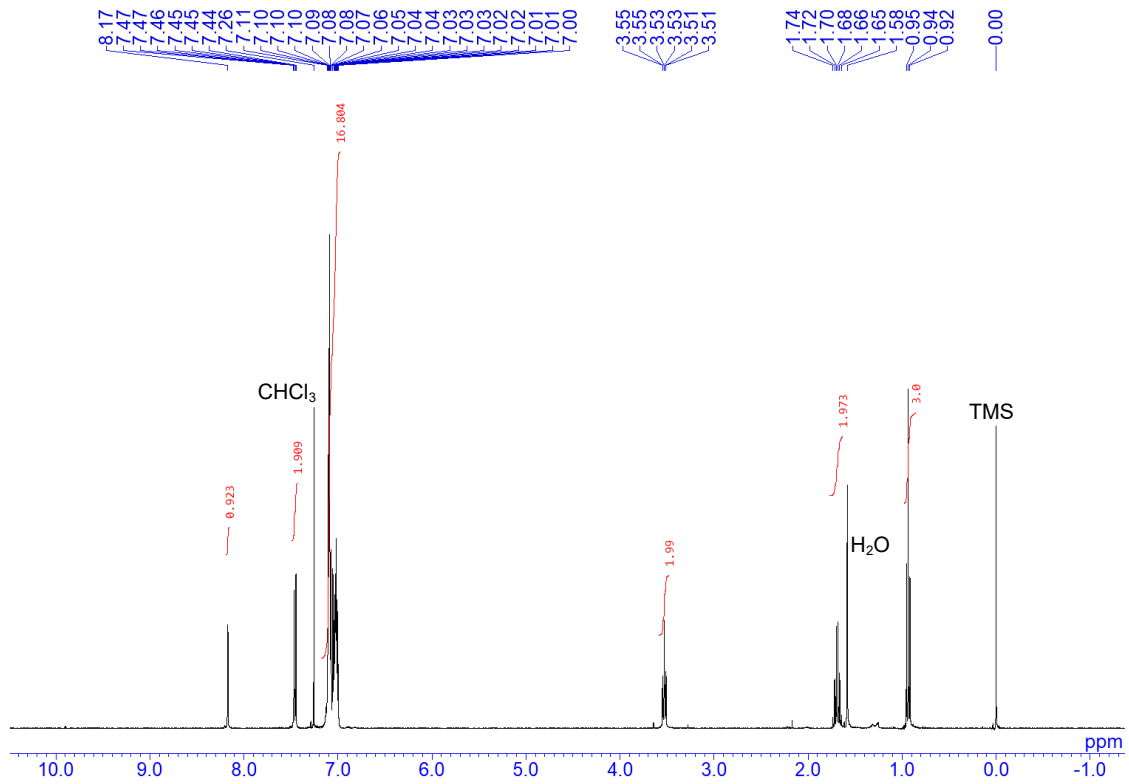

Chart S4. ^{1}H NMR spectrum of **TPE-Pr** in $CDCl_3$.

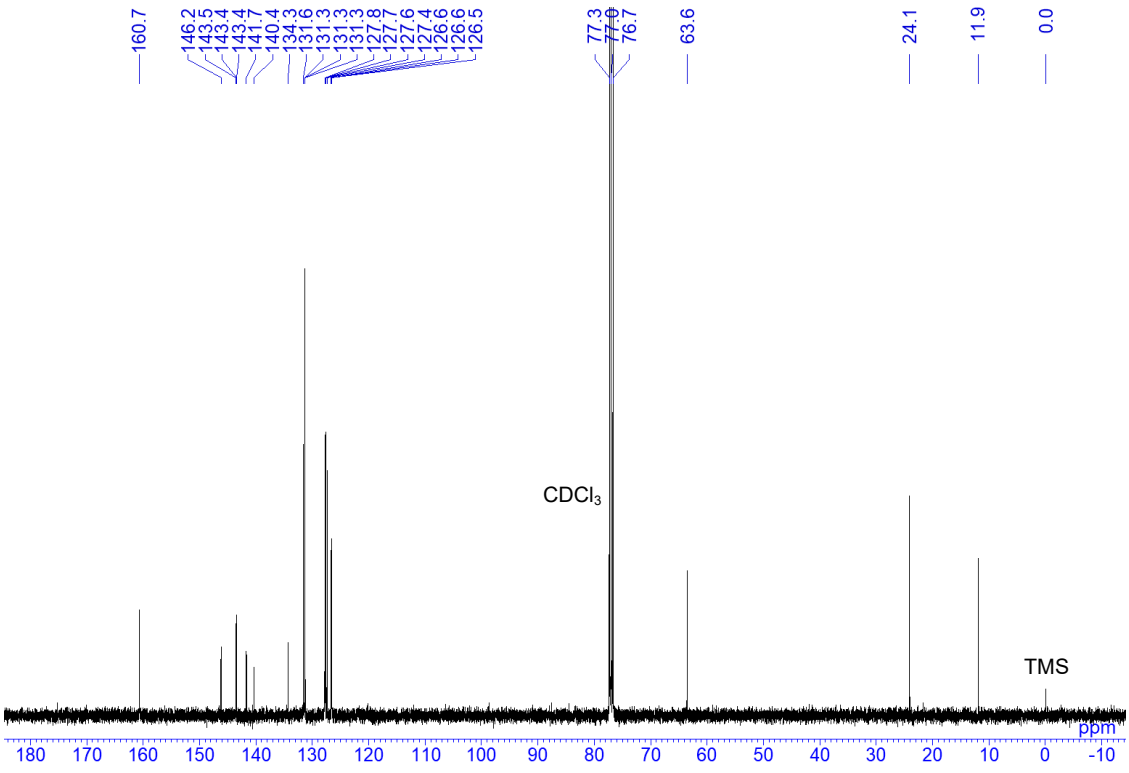

Chart S5. ^{13}C NMR spectrum of **TPE-Pr** in $CDCl_3$.

Synthesis of MEH-PPV

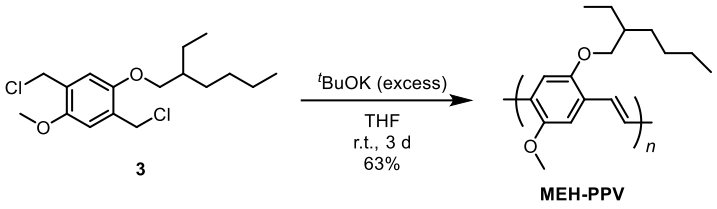

A solution of 1,4-bis(chloromethyl)-2-(2′-ethylhexyloxy)-5-methoxybenzene (**3**) (15.9 g, 47.6 mmol) in THF (800 mL) was stirred under N_2 atmosphere. The solution of *tert*-BuOK (24.0 g, 214 mmol) in THF (1200 mL) was added dropwise to this stirred colorless solution. The mixture was stirred at room temperature under N_2 atmosphere for 3 d. Then, the orange gel-like solution was diluted with excess THF and reprecipitated into MeOH. The residue was washed with hexane, MeOH and acetone, and then, extracted with $CHCl_3$ by Soxhlet extractor to afforded **MEH-PPV** (7.76 g, 63%) as a red solid. This reaction was carried out twice to obtain different molecular weight polymers. The molecular weights were determined by GPC with polystyrene standards with chloroform as an eluent. The first one was M_n = 64,000 and M_w/M_n = 4.8, and that of the second one was M_n = 114,000 and M_w/M_n = 3.7.

^{1}H NMR ($CDCl_3$, 400 MHz) δ 7.52 (br, 1H), 7.19 (br, 1H), 3.95 (m, 5H), 1.83 (br, 1H), 1.54–1.25 (m, 8H), 1.00 (t, J = 7.1 Hz, 3H), 0.91 (t, J = 6.1 Hz, 3H) ppm; ^{13}C NMR ($CDCl_3$, 100 MHz) δ 151.4, 71.3, 56.5, 39.9, 39.8 30.9, 30.9, 29.7, 29.3, 29.2, 24.3, 23.1, 14.1, 11.5, 11.4, 11.4, 11.4 ppm.

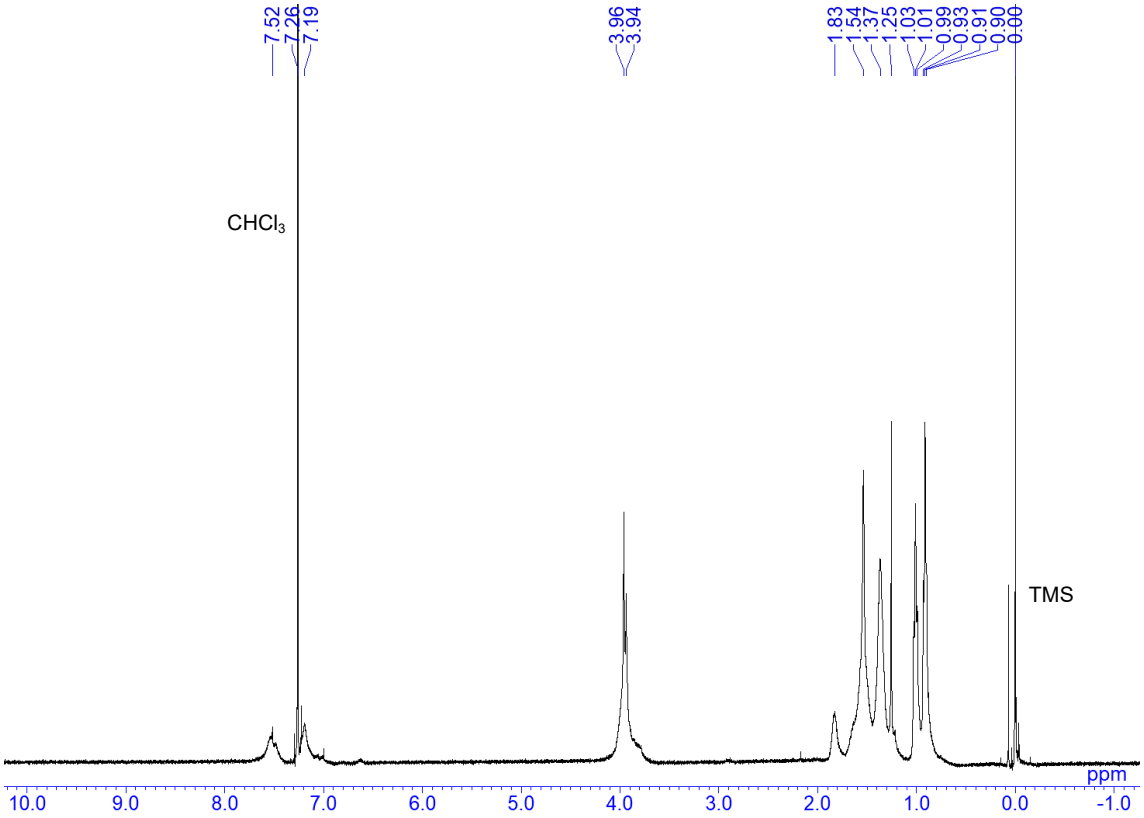

Chart S6. ^{1}H NMR spectrum of **MEH-PPV** in $CDCl_3$.

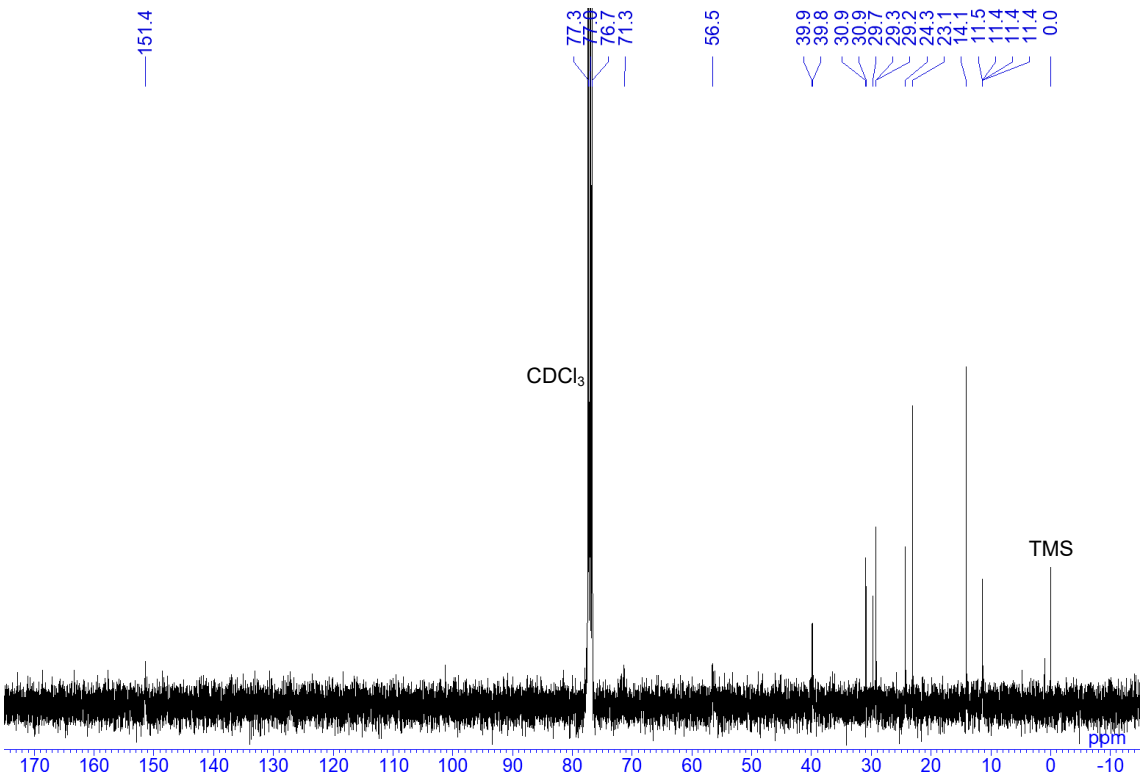

Chart S7. ^{13}C NMR spectrum of **MEH-PPV** in $CDCl_3$.

SEM observations

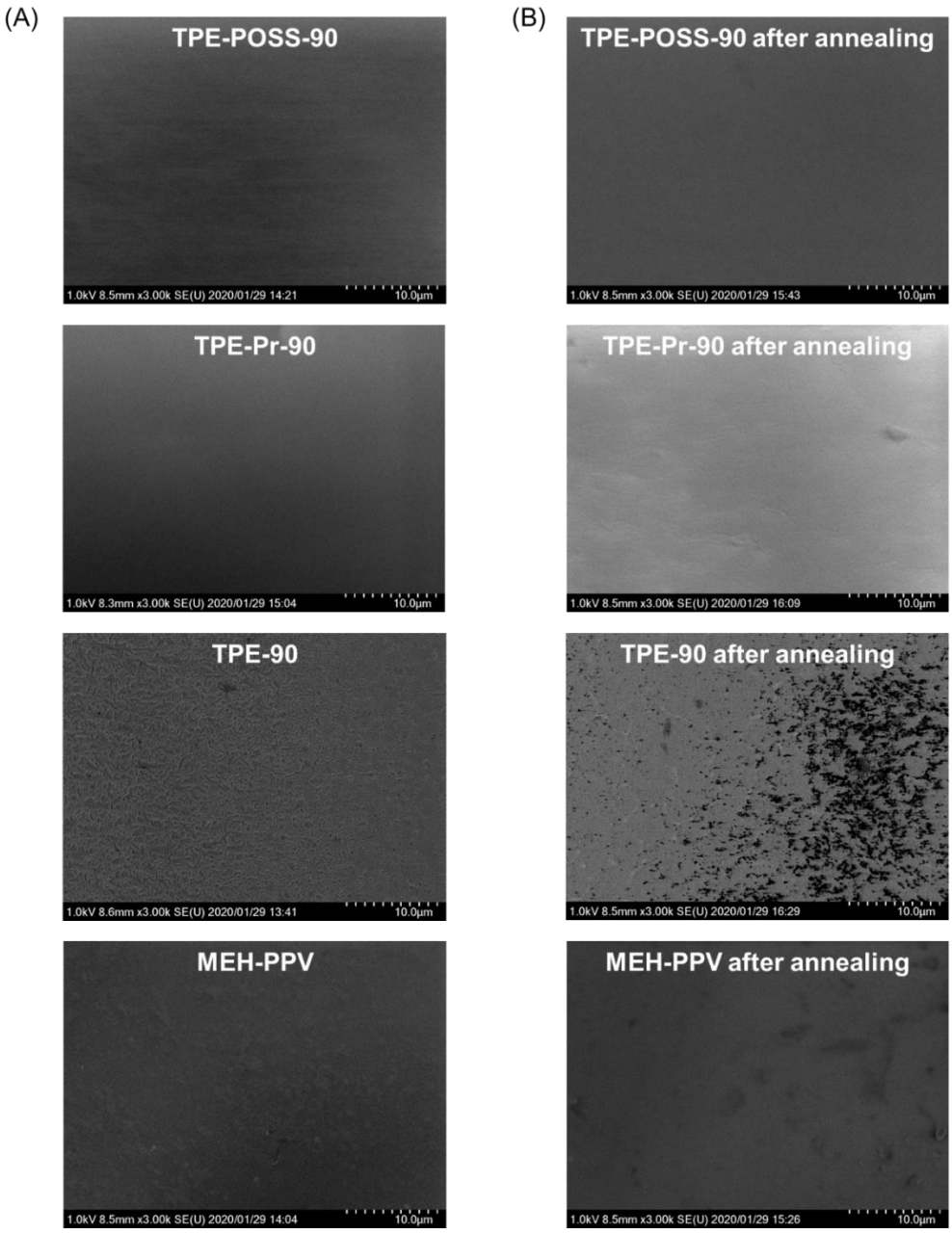

Figure S1. (A) SEM images of **TPE-POSS-90**, **TPE-Pr-90**, **TPE-90** and **MEH-PPV** before (left) and (B) after annealing (right). The films were prepared by a spin coating method (1000 rpm, 30 s) on the ITO substrates and then, the films were dried in vacuo for 12 h. Annealing was carried out at 60 ºC for 12 h under vacuum condition. Before annealing, **TPE-POSS-90** and **TPE-Pr-90** were homogeneous, however **TPE-90** and **MEH-PPV** were heterogeneous. After annealing, **TPE-Pr-90** was slightly phase separated, meanwhile **TPE-POSS-90** preserved the homogeneous image. The molecular weight of using **MEH-PPV** was M_n = 114,000, M_w/M_n = 3.7.

Optical data of compounds in solution and film states

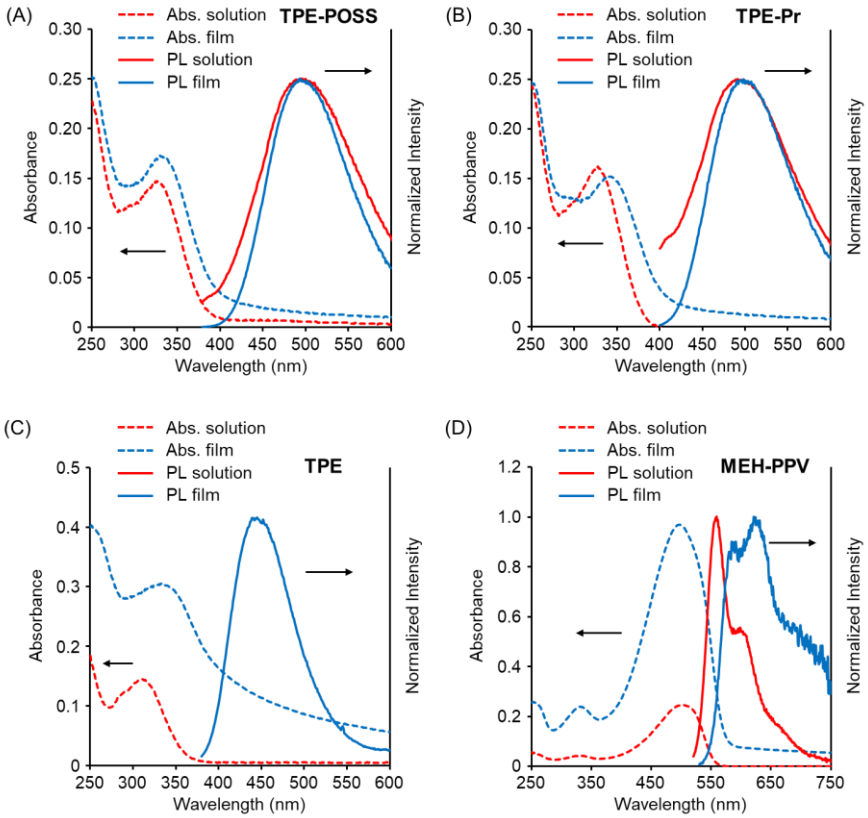

Figure S2. UV–vis and PL spectra of (A) **TPE-POSS**, (B) **TPE-Pr**, (C) **TPE** and (D) **MEH-PPV** in solution ($CHCl_3$, 1.0×10^{-6} M for **TPE-POSS**, 1.0×10^{-5} M for **TPE-Pr**, **TPE** and 1.0×10^{-5} M per repeating unit for **MEH-PPV**) and film states (prepared by a spin-coating method (1000 rpm, 30 s) from $CHCl_3$ solution (1.0 mg/300 μL)), excited at the wavelength of absorption maxima. The molecular weight of using **MEH-PPV** was M_n = 64,000, M_w/M_n = 4.8.

Table S1. Optical data of pristine compounds in solution and film states

	solution[a]			film[b]		
	λ_{abs} (nm)	λ_{PL} (nm)	Φ_{PL} (%)	λ_{abs} (nm)	λ_{PL} (nm)	Φ_{PL} (%)
TPE-POSS	326	496	<1.0	330	494	31
TPE-Pr	328	491	<1.0	342	498	20
TPE	311	n.d.[c]	n.d.[c]	332	445	20
MEH-PPV	503	559	31	497	591, 621	6.5

[a] In $CHCl_3$, 1.0×10^{-6} M for **TPE-POSS**, 1.0×10^{-5} M for **TPE-Pr**, **TPE** and 1.0×10^{-5} M per repeating unit for **MEH-PPV**. Excited at the wavelengths of absorption maxima (λ_{abs}).

[b] Prepared by a spin-coating method (1000 rpm, 30 s) from $CHCl_3$ solution (1.0 mg/300 μL).

[c] Not detected.

Liner relationships of content ratios and absorbances

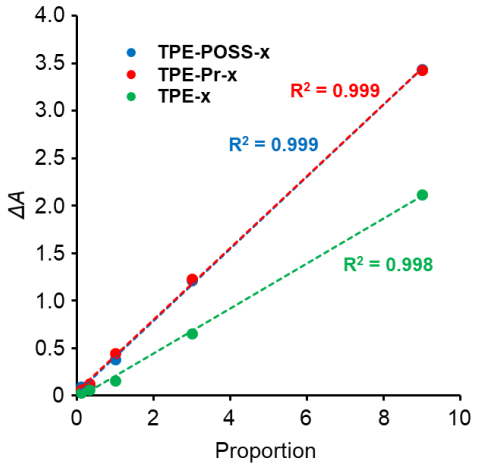

Figure S3. Linearity between *ΔA* and content proportion of TPE derivatives to **MEH-PPV** in the hybrid films. The plotted values were listed in Table S1. Decision coefficient (R^2) is described in the figure. The molecular weight of using **MEH-PPV** was M_n = 64,000, M_w/M_n = 4.8.

Table S2. The summary of spectroscopic data calculated from Figure 4.

x	0	10	25	50	75	90
Proportion[a]	0	0.11	0.33	1	3	9
TPE-POSS-x[b]	0	0.097	0.12	0.39	1.21	3.44
TPE-Pr-x[b]	0	0.061	0.13	0.45	1.23	3.43
TPE-x[c]	0	0.036	0.067	0.16	0.65	2.12

[a] Proportion was calculated by the equation of (content ratio of TPE derivatives / **MEH-PPV**).

[b] The difference of normalized absorbance (normalized at 500 nm, the value = 1) at 330 nm, $\Delta A = A$(x wt%) − A(0 wt%).

[c] The difference of normalized absorbance (normalized at 500 nm, the value = 1) at 320 nm, $\Delta A = A$(x wt%) − A(0 wt%).

The detail method for estimation of the relative PL spectra

Relative peak intensity (I_R) was estimated with the equation (1). The relative PL spectrum is drawn using the $I_R(\lambda)$ of each hybrid film. I_R reflected the maximum performance of the prepared hybrid film if entire of the hybrid film was homogeneously excited and the resulted emission was perfectly detected. The parameters calculated from Figures 1, S3 to S5 and Table 1 are shown in Tables S2 to S5. The molecular weight of using **MEH-PPV** was M_n = 64,000, M_w/M_n = 4.8.

$$I_R(\lambda) = kI_x(\lambda) \qquad k = \frac{(A_x/A_0) \times (\Phi_{PL,x}/\Phi_{PL,0})}{S_x/S_0} \qquad \text{(1)}$$

k: correction coefficient

A_x: experimental absorbance at excitation wavelength in x wt% film

$\Phi_{PL,x}$: absolute photoluminescence quantum yield in x wt% film

S_x : surface area of experimental PL spectrum with wavenumber in x wt% film

$I_x(\lambda)$: intensity of experimental PL spectrum at each wavelength (λ) in x wt% film

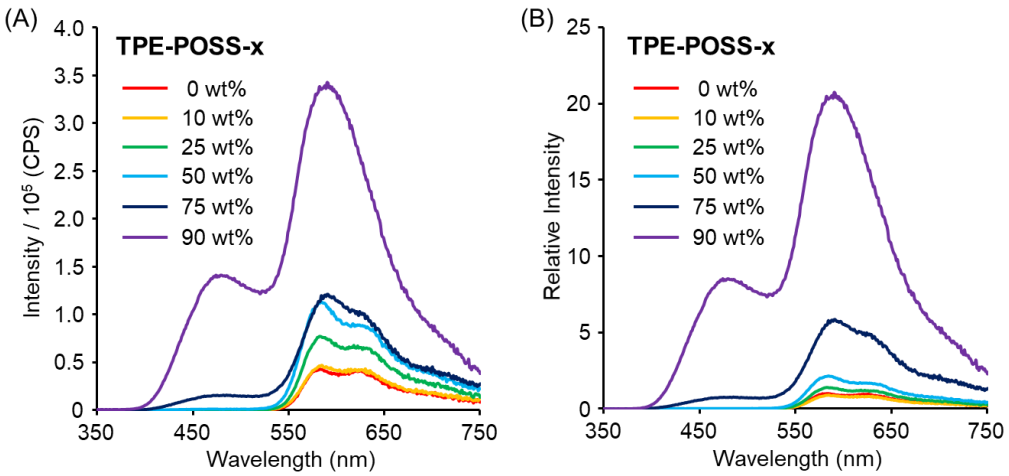

Figure S4. (A) Experimental and (B) relative PL spectra of the hybrid films of **TPE-POSS-x** excited at 330 nm.

Table S3. Parameters for estimation of relative PL spectra of the hybrid films of **TPE-POSS-x**

x	0	10	25	50	75	90
A_x/A_0[a]	1	0.95	1.4	2.1	4.9	15.5
S_x/S_0	1	1.1	1.7	2.5	3.1	10
$\Phi_{PL,x}/\Phi_{PL,0}$[b]	1	0.92	0.95	0.97	1.3	1.7
k	1	0.80	0.76	0.82	2.1	2.6

[a] At 330 nm.

[b] Excited at 330 nm.

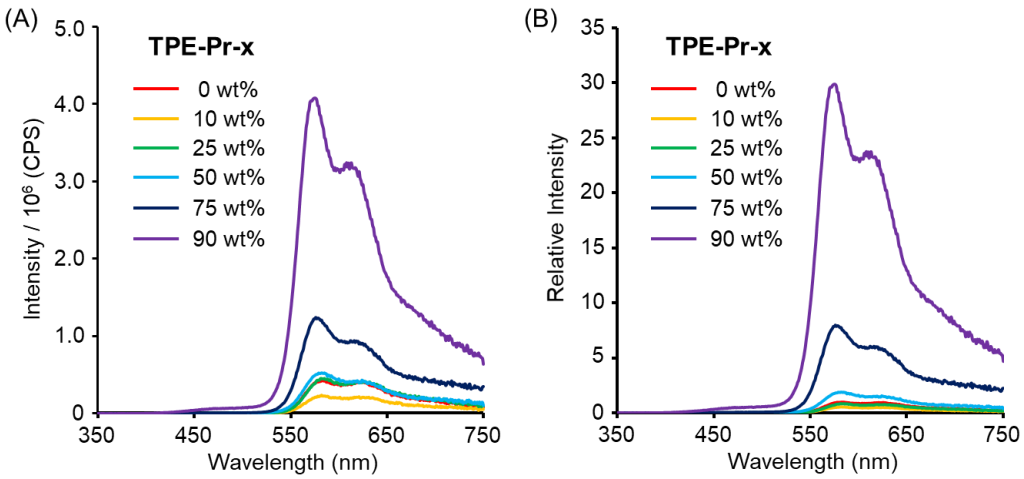

Figure S5. (A) Experimental and (B) relative PL spectra of the hybrid films of **TPE-Pr-x** excited at 330 nm.

Table S4. Parameters for estimation of relative PL spectra of the hybrid films of **TPE-Pr-x**

x	0	10	25	50	75	90
A_x/A_0[a]	1	0.80	1.1	2.2	5.3	11
S_x/S_0	1	0.54	1.1	1.2	2.7	8.5
$\Phi_{PL,x}/\Phi_{PL,0}$[b]	1	0.71	0.77	0.79	1.4	2.4
k	1	1.1	0.80	1.5	2.8	3.1

[a] At 330 nm.

[b] Excited at 330 nm.

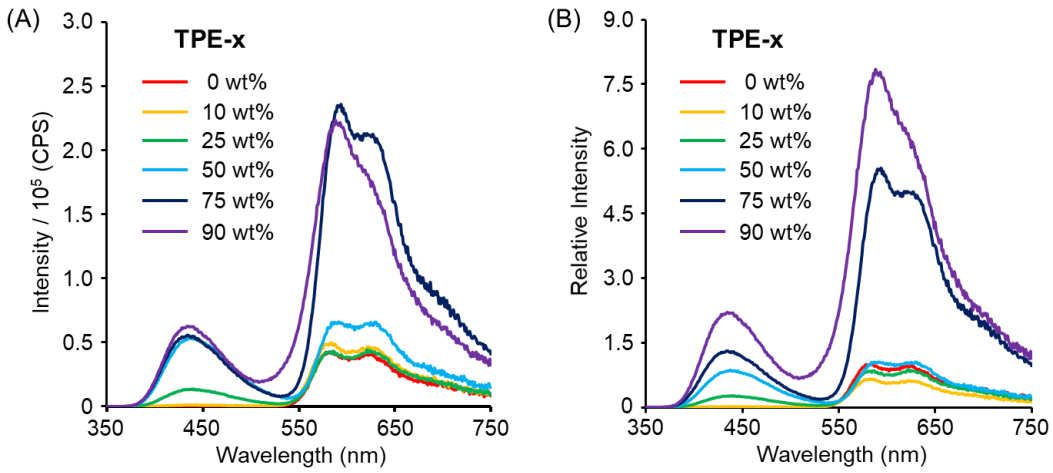

Figure S6. (A) Experimental and (B) relative PL spectra of the hybrid films of **TPE-x** excited at 330 nm.

Table S5. Parameters for estimation of relative PL spectra of the hybrid films of **TPE-x**

x	0	10	25	50	75	90
A_x/A_0[a]	1	0.76	1.0	1.6	3.7	6.0
S_x/S_0	1	1.2	1.3	2.4	6.0	5.8
$\Phi_{PL,x}/\Phi_{PL,0}$[b]	1	0.89	1.1	1.0	1.6	1.4
k	1	0.57	0.84	0.68	1.0	1.5

[a] At 330 nm.

[b] Excited at 330 nm

Fluorescence resonance energy transfer (FRET) efficiency

Table S6. FRET efficiency of the hybrid films of **TPE-POSS-x** [a]

x	10	25	50	75	90
Φ_d [b]	31.1	31.1	31.1	31.1	31.1
Φ_{da} [c]	0	0	0	0.2	1.5
E [d]/%	100	100	100	99.4	95.2

[a] **MEH-PPV** (M_n = 64,000, M_w/M_n = 4.8)

[b] Absolute photoluminescence quantum efficiency of only a donor (**TPE-POSS-100**), excited at 330 nm.

[c] Absolute photoluminescence quantum efficiency of a donor (**TPE-POSS-x**) including an acceptor (**MEH-PPV**), excited at 330 nm and integrated from 380 ~ 535 nm.

[d] FRET energy transfer (E): $E = 1-\Phi_{da}/\Phi_d$

Table S7. FRET efficiency of the hybrid films of **TPE-Pr-x** [a]

x	10	25	50	75	90
Φ_d [b]	20.2	20.2	20.2	20.2	20.2
Φ_{da} [c]	0	0	0	0	0
E [d]/%	100	100	100	100	100

[a] **MEH-PPV** (M_n = 64,000, M_w/M_n = 4.8)

[b] Absolute photoluminescence quantum efficiency of only a donor (**TPE-Pr-100**), excited at 330 nm.

[c] Absolute photoluminescence quantum efficiency of a donor (**TPE-Pr-x**) including an acceptor (**MEH-PPV**), excited at 330 nm and integrated from 380 ~ 535 nm.

[d] FRET energy transfer (E): $E = 1-\Phi_{da}/\Phi_d$

Table S8. FRET efficiency of the hybrid films of **TPE-x** [a]

x	10	25	50	75	90
Φ_d [b]	19.8	19.8	19.8	19.8	19.8
Φ_{da} [c]	0	0.2	0.8	0.5	0.9
E [d]/%	100	99.0	96.0	97.5	95.4

[a] **MEH-PPV** (M_n = 64,000, M_w/M_n = 4.8)

[b] Absolute photoluminescence quantum efficiency of only a donor (**TPE-100**), excited at 330 nm.

[c] Absolute photoluminescence quantum efficiency of a donor (**TPE-x**) including an acceptor (**MEH-PPV**), excited at 330 nm and integrated from 380 ~ 535 nm.

[d] FRET energy transfer (E): $E = 1-\Phi_{da}/\Phi_d$

Excitation spectra

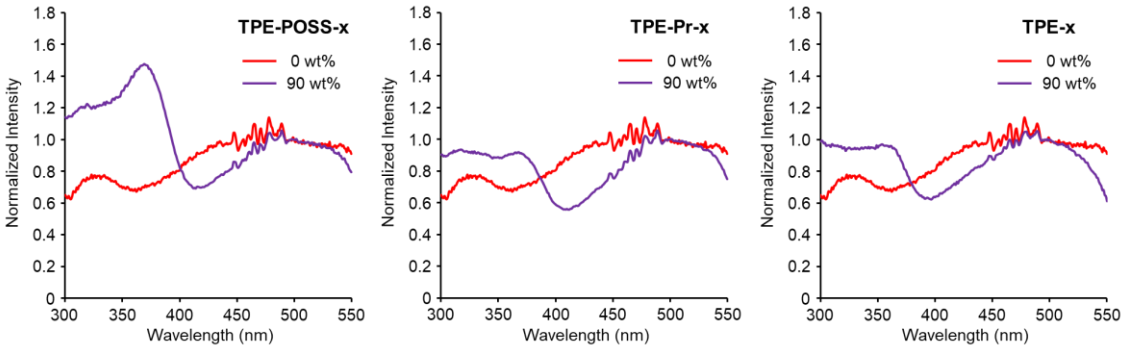

Figure S7. Excitation spectra of hybrid films, **TPE-POSS-x**, **TPE-Pr-x** and **TPE-x**, monitored at 580 nm. The spectra were normalized at 500 nm which was the absorption of only **MEH-PPV**. The contribution of the TPE derivatives were confirmed by the fact that the ratios of the intensity of **TPE-POSS-90**, **TPE-Pr-90** and **TPE-90** at around 330 nm to that of **MEH-PPV** at 500 nm increased in comparison to that of the pristine **MEH-PPV** film, respectively. The molecular weight of using **MEH-PPV** was M_n = 64,000, M_w/M_n = 4.8.

CIE diagrams

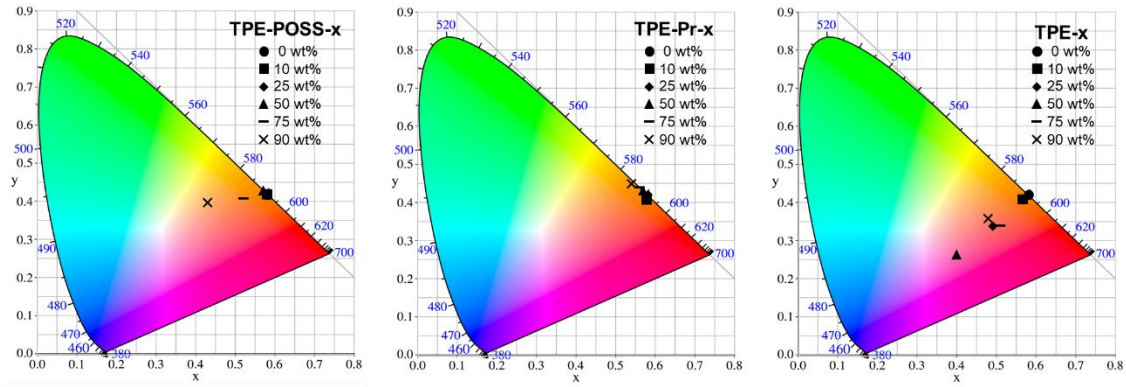

Figure S8. CIE diagrams of hybrid films, **TPE-POSS-x**, **TPE-Pr-x** and **TPE-x**, excited at 330 nm. The parameters are shown in Table S6. The molecular weight of using **MEH-PPV** was M_n = 64,000, M_w/M_n = 4.8.

Table S9. CIE coordinates (x, y) of hybrid films with **MEH-PPV** (M_n = 64,000, M_w/M_n = 4.8), **TPE-POSS-x**, **TPE-Pr-x** and **TPE-x**, excited at 330 nm

x	0	10	25	50	75	90
TPE-POSS-x	(0.58, 0.42)	(0.58, 0.42)	(0.58, 0.42)	(0.57, 0.43)	(0.52, 0.41)	(0.43, 0.40)
TPE-Pr-x	(0.58, 0.42)	(0.58, 0.42)	(0.58, 0.41)	(0.57, 0.43)	(0.56, 0.44)	(0.54, 0.45)
TPE-x	(0.58, 0.42)	(0.57, 0.41)	(0.49, 0.34)	(0.40, 0.26)	(0.51, 0.34)	(0.48, 0.36)

UV–vis absorption spectra before and after annealing

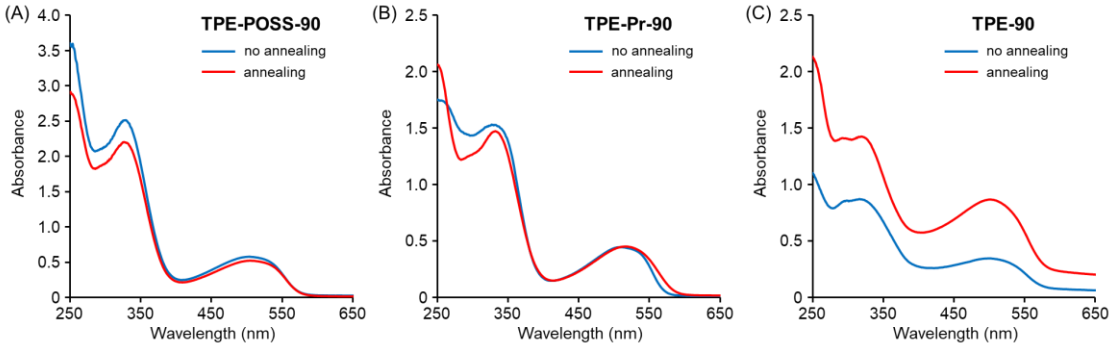

Figure S9. UV–vis absorption spectra of (A) **TPE-POSS-90**, (B) **TPE-Pr-90** and (C) **TPE-90** before and after annealing. Annealing was carried out at 60 ºC for 12 h under vacuum condition.

UV–vis absorption and relative PL spectra of MEH-PPV before and after annealing

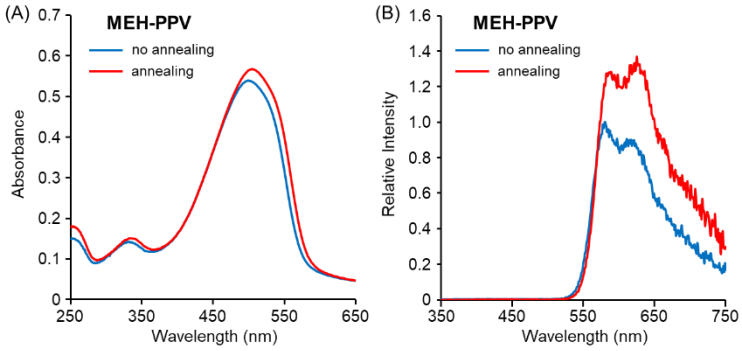

Figure S10. (A) UV–vis absorption spectra and (B) relative PL spectra of **MEH-PPV** before and after annealing. Annealing was carried out at 60 ºC for 12 h under vacuum condition. The molecular weight of using **MEH-PPV** was M_n = 114,000, M_w/M_n = 3.7.

Variable temperature (VT) PL spectra of hybrid materials and MEH-PPV

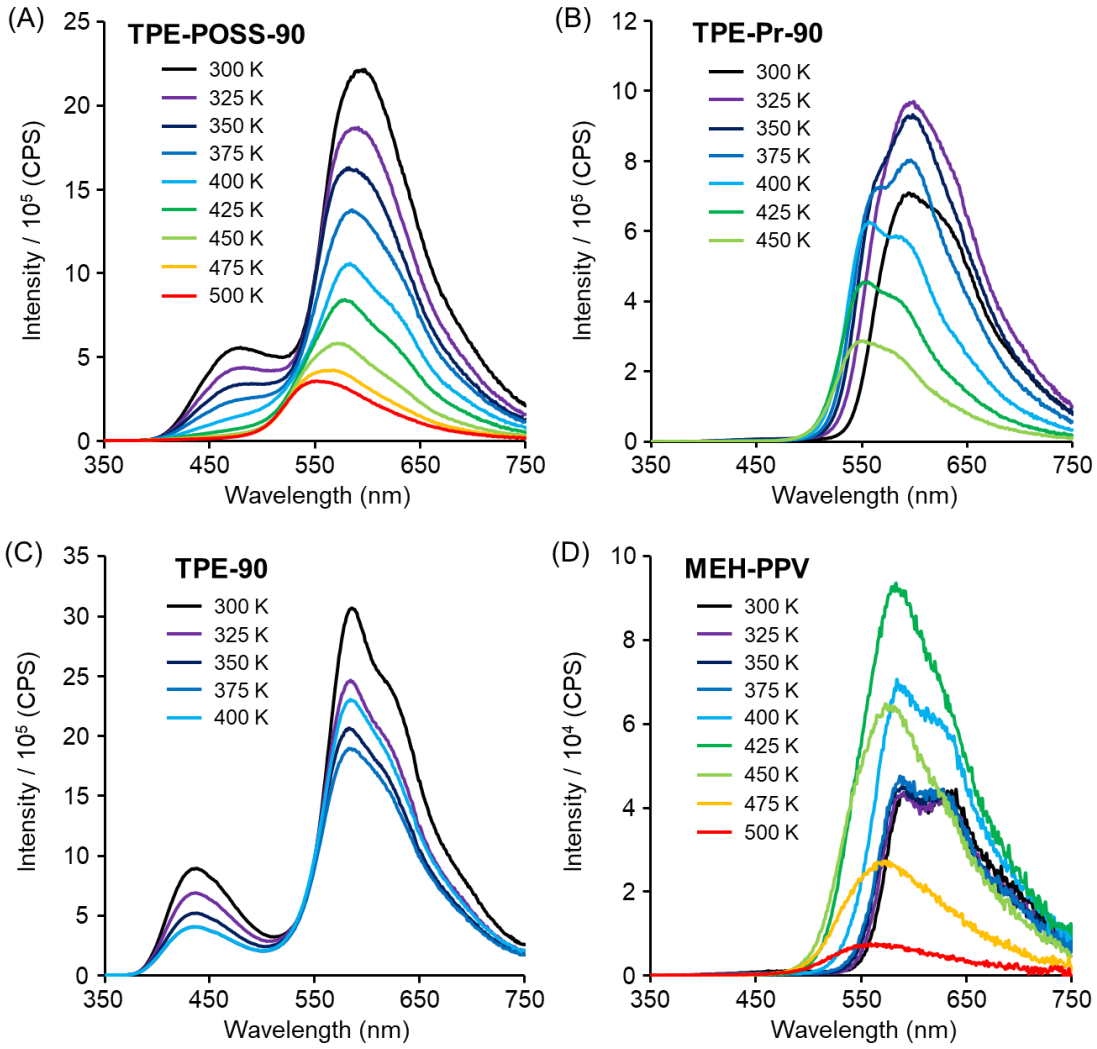

Figure S11. Variable temperature (VT) PL spectra of (A) **TPE-POSS-90**, (B) **TPE-Pr-90**, and (C) **TPE-90** and (D) **MEH-PPV** under N_2 atmosphere. The molecular weight of using **MEH-PPV** was M_n = 114,000, M_w/M_n = 3.7.

Analysis of VT PL spectra of hybrid materials and MEH-PPV

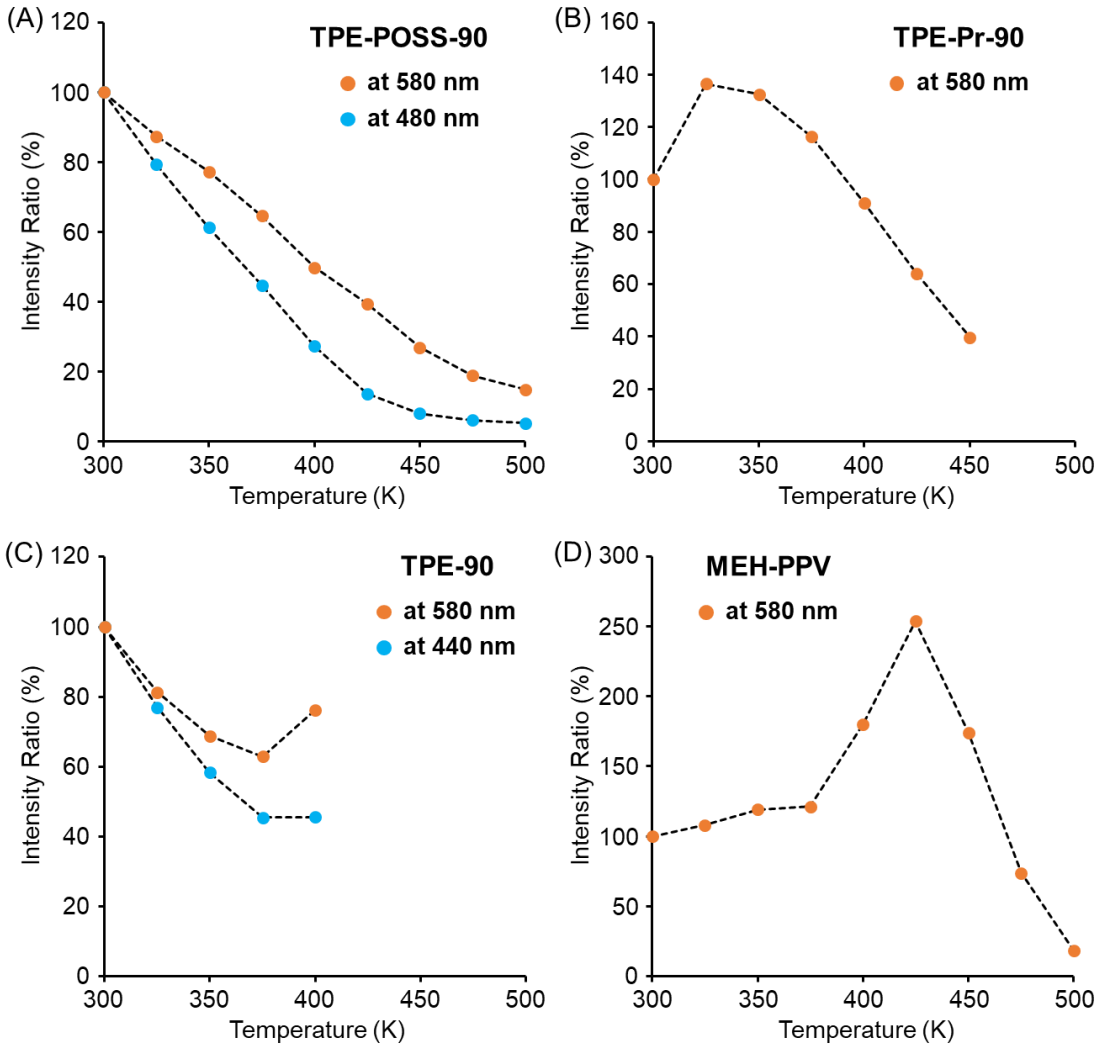

Figure S12. Intensity ratio of VT PL spectra of (A) **TPE-POSS-90**, (B) **TPE-Pr-90**, and (C) **TPE-90** and (D) **MEH-PPV**. The intensity was monitored at 480 and 580 nm for **TPE-POSS-90**, at 580 nm for **TPE-Pr-90**, at 440 and 580 nm for **TPE-90**, at 480 nm for **MEH-PPV**. The VT measurement was started at 300 K and the temperature increased before a decomposition point determined from a TGA measurement. The intensity at 300 K was set as standard intensity, 100%. The molecular weight of using **MEH-PPV** was M_n = 114,000, M_w/M_n = 3.7.

VT PL spectra of TPE-POSS-98

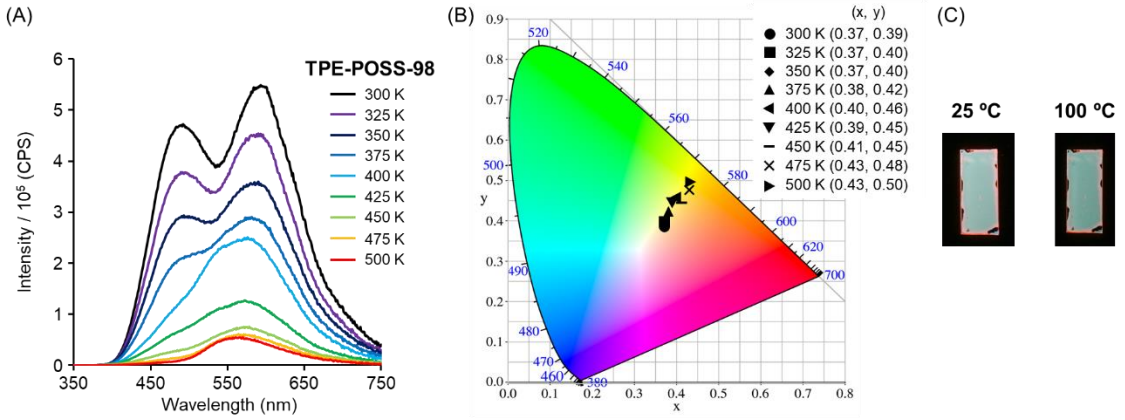

Figure S13. (A) VT PL spectra, (B) CIE diagram and (C) photos under heating (excited by UV lamp (365 nm)) of **TPE-POSS-98** under N_2 atmosphere. The molecular weight of using **MEH-PPV** was M_n = 114,000, M_w/M_n = 3.7.

Repeatability of VT PL spectra of TPE-POSS-90

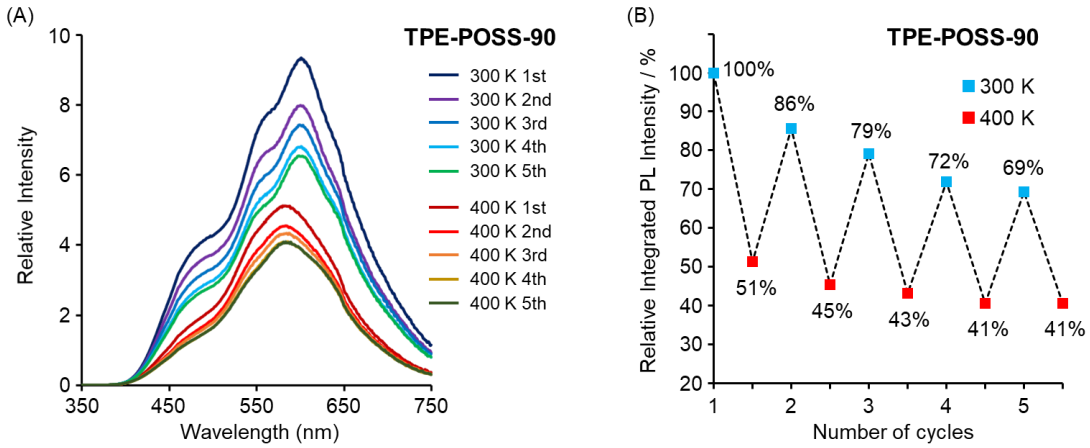

Figure S14. Repeatability of VT PL spectra of **TPE-POSS-90** monitored at 300 and 400 K during five heating and cooling cycles with 10 min holding time after annealing at 400 K for 10 min under N_2 atmosphere. (A) Relative PL spectra and (B) relative integrated PL intensity. Relative percentage of each cycle and temperature was estimated based on the integrated PL intensity at 300 K (1st cycle) being 100%. The molecular weight of using **MEH-PPV** was M_n = 114,000, M_w/M_n = 3.7.

Thermal degradation PL spectra of TPE-POSS-90 at 400 K

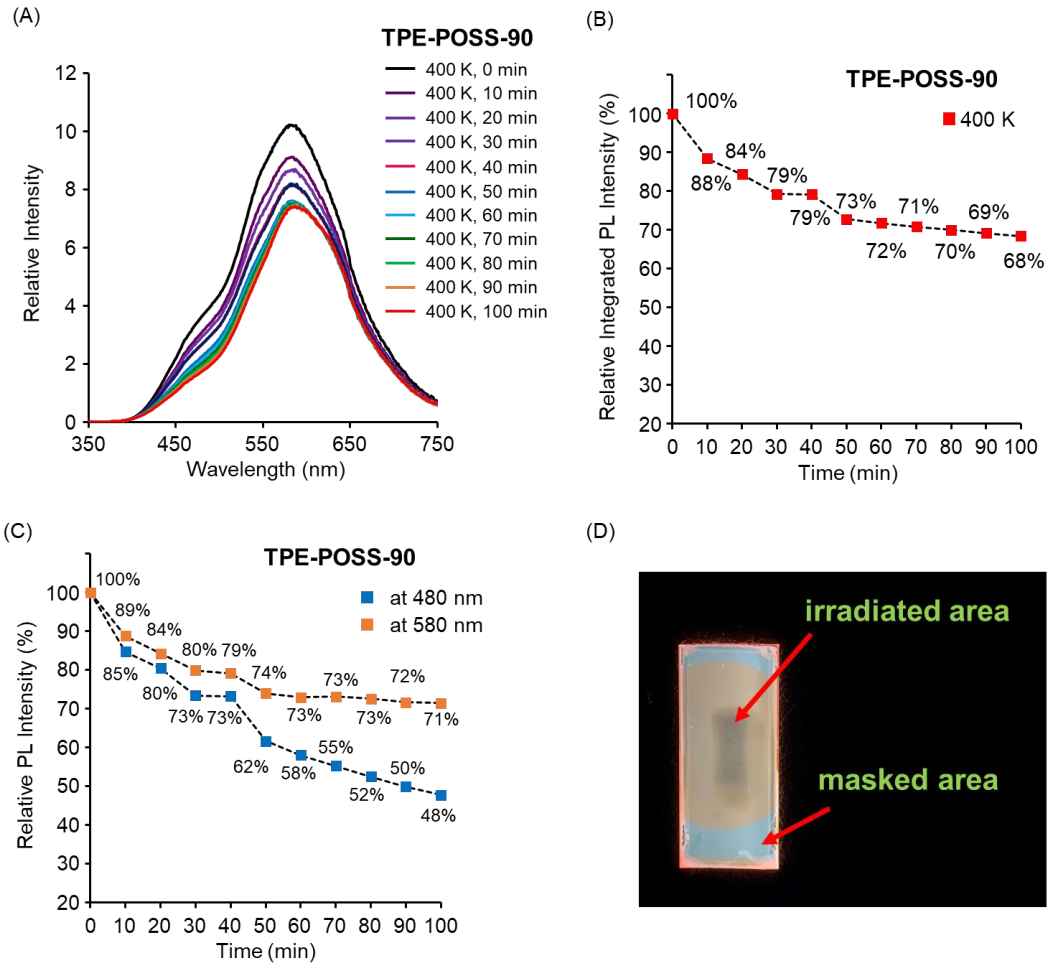

Figure S15. (A) Thermal degradation PL spectra of **TPE-POSS-90** monitored at 400 K after annealing at 400 K for 10 min under N_2 atmosphere. (B) Relative integrated intensity of PL spectra. Relative percentage of each time was estimated based on the integrated PL intensity at 400 K (0 min) being 100%. (C) Relative PL intensity monitored at 480 nm and 580 nm. Relative percentage of each time was estimated based on the PL intensity at 400 K (0 min) being 100%. (D) Photo of **TPE-POSS-90** after the thermal degradation test. It was clearly observed that the intensity of irradiated area decreased and the color partially became orange. In contrast, masked area still showed white-light emission after the thermal degradation test. The photo was pictured under UV irradiation (365 nm). The molecular weight of using **MEH-PPV** was M_n = 114,000, M_w/M_n = 3.7.